Identification and characterization of C-terminal alterations in *Arabidopsis thaliana* FATTY ACID DESATURASE 6 (FAD6)

by

Hannah J. Lusk

B.S., Kansas State University, 2019

A THESIS

submitted in partial fulfillment of the requirements for the degree

MASTER OF SCIENCE

Department of Biochemistry and Molecular Biophysics
College of Arts and Sciences

KANSAS STATE UNIVERSITY
Manhattan, Kansas

2019

Approved by:

Major Professor
Ruth Welti

Copyright

Abstract

Lipid analysis of leaves from the Arabidopsis T-DNA insertion line Salk_109175C revealed a decreased ratio between two monogalactosydiacylglycerol molecular species, MGDG(18:3/16:3) and MGDG(18:3/18:3), as well as other alterations consistent with a disruption in chloroplast glycerolipid assembly. Salk_109175C has a confirmed insertion in the At5g64790 locus which did not co-segregate with the lipid phenotype in the F2 generation of a wild type (Col-0) x Salk_109175C cross. The mutation associated with the lipid alterations mapped to the At4g30950 locus, which encodes for the plastidial ω6 desaturase FATTY ACID DESATURASE 6 (FAD6). Sequencing revealed a splice site mutation between exons 9 and 10, which leads to the in-frame deletion of 13 amino acids near the C-terminal end of the protein. Sequence comparison across species revealed multiple amino acids within the deletion are conserved in all plants, and even cyanobacteria. We cloned and heterologously co-expressed several constructs of *AtFAD6* with photosynthetic ferredoxin (*AtFD2*) under the control of a constitutive promoter (CDC11) or an inducible promoter (Gal1/10) in yeast, with the goal of determining which combination of gene and promoter results in the highest activity. The future of this project involves using this system to clone and express mutant *fad6* constructs in yeast to evaluate the impact of conserved residues on enzyme function.

Table of Contents

List of Figures

List of Tables

Acknowledgements

I would like to acknowledge Mary Roth for her help in acquiring and interpreting data from the mass spectrometer, Sunitha Shiva for her mass spectrometry expertise and ideas, Libin Yao for help with GC-FID and GC-MS data acquisition, Pamela Tamura for her guidance and help with plant growth and lipid extraction, Madeline Colter for performing the initial lipid screen that identified this mutant, Sujon Sarowar for initial genetic analysis of Salk_109175C, Zulkarnain Chowdhury for guiding me through the process of map-based cloning, Prasad Parchuri for his help with cloning the Arabidopsis *FAD6* desaturase into yeast, and Nick Neumann for his advice with cloning and for his continuing work on this project. Additionally, I would like to thank Jyoti Shah for advice with mapping and for inviting me to learn map-based cloning in his lab under the guidance of one of his post-doctoral fellows, as well as Gregory Finnigan for his guidance with designing constructs and cloning the *FAD6* desaturase into yeast. Most importantly, I would like to thank Ruth Welti for taking me under her wing as an undergraduate and encouraging me to pursue a master's degree in her lab, in addition to Timothy Durrett and Kathrin Schrick for serving on my supervisory committee and for their guidance over the course of this work.

Chapter 1 - Introduction and Literature Review

Lipids and Lipidomics

Lipids are small, hydrophobic biomolecules that play important roles in biological membranes, signal transduction, and energy storage. Eukaryotic cells are thought to contain billions of lipid molecular species, each with unique chemical and physical properties [1]. Other macromolecules, such as proteins and nucleic acids, are defined by their structural components; nucleic acids are made from linear combinations of four nucleotides, and proteins from 20 amino acids. Lipids, on the other hand, are broadly defined as small molecules that are amphipathic or hydrophobic in nature. Anything soluble in organic (nonpolar) solvents is classified as a lipid, and lipids are the most structurally diverse class of biological macromolecules.

According to the Lipid Metabolites and Pathways Strategy (LIPID MAPS) classification system developed by the LIPID MAPS consortium, lipid molecular species can be separated into eight categories based on the subunits from which they are derived and other structural characteristics[2]. Lipids can be classified as fatty acyls, glycerolipids, phospholipids, sphingolipids, saccharolipids and polyketides (derived from ketoacyl subunits), and sterol lipids or prenol lipids (derived from isoprene subunits). Each of these categories can be further divided into numerous different classes and subclasses[2]. Due to challenges with structural elucidation, there are no reliable estimates for the number of distinct lipid structures that arise in nature, but given the importance of these compounds in many biological processes, it is imperative that scientists continue working to profile the lipids of diverse organisms and resolve the technical challenges associated with structural elucidation and quantification[2].

The term “metabolome” refers to the collection of all small molecules found in a cell or tissue, including lipids, nucleotides, amino acids, sugars, and intermediary metabolites. “Lipidome” refers to the complete lipid profile of a cell or tissue; it is composed of all the component lipid molecular species including those that exist as small molecules, and those that are incorporated into macromolecules. Lipidomics, the comprehensive analysis of lipid molecules within biological systems, is a field, which has experienced recent growth due to advances in analytical technologies, including mass spectrometry (MS) and computational methods[2]. There has also been increased recognition of the important roles lipids play in essential biological processes, particularly in signaling, and in common human diseases including obesity, stroke, hypertension, and diabetes[2].

Analysis of the molecular species within crude lipid extracts can be achieved using a variety of techniques, depending on the information desired. Often researchers opt to separate complex mixtures into individual lipid classes using chromatography techniques prior to detection and quantification. Historically, chromatography techniques, including normal-phase thin-layer chromatography (TLC) on silica, have been employed to separate classes of glycerolipids, glycerophospholipids, and sphingolipids based primarily on the polarity of these complex lipids. TLC combined with a colorimetric assay to analyze phosphorus content, can be employed to separate and quantify the phospholipid classes within a given sample[3-8]. Alternatively, following TLC, gas-liquid chromatography (GC) of simple lipid derivatives can be used to detect and quantify the fatty acids or other simple lipids making up each lipid class. Despite its utility in separating lipid classes, normal-phase TLC is nearly useless for separating individual lipid molecular species within classes. With the advent of normal- and reverse-phase high-

performance liquid chromatography (HPLC), complex lipids could be separated into both head group classes and lipid molecular species within those classes. After separation by HPLC, these molecular species could be quantified by integration of peak area from UV detection, although response factors vary among species, or by evaporative light scattering. However, these detectors (UV and evaporative light scattering) are limited in their ability to detect and quantify low abundance lipid species, which often play key roles in biological processes such as signal transduction. Addition of mass spectrometry detectors, beginning with fast atom bombardment/MS in the 1980's and combinations of HPLC with mass spectrometry led to substantial advances[9].

Technological insufficiencies in the field of lipid analysis left room for the advent of new methods. The utility of a mass spectrometer with an electrospray ionization source (ESI-MS) for lipid analysis was first demonstrated by Weintraub et al. (1991) and Duffin et al. (1991) who utilized it in in the analyses of platelet activating factor and diacylglycerols, respectively[10,11]. Mass spectrometry-based techniques that involve direct infusion and detection without prior separation, such as ESI-MS, provide an advantage over approaches involving multiple separations because they are less time consuming and sensitive enough to detect low abundance lipid species, which means for most biological samples less than 1 mg of tissue dry weight is required for a comprehensive analysis[12]. Many techniques based on ESI-MS have been developed and exploited for the analysis of diverse lipid classes, subclasses, and individual molecular species from crude lipid extracts. Early on, Han and Gross developed a direct-infusion approach that takes advantage of the scanning capabilities of a single quadrupole mass spectrometer. For this procedure, originally used on animal extracts, negative ion mode is used to

analyze phosphatidylglycerol (PG), phosphatidylinositol (PI), phosphatidylserine (PS), phosphatidic acid (PA), and sulfatide species. Then, after the addition of lithium ions, positive mode is used to detect phosphatidylcholine (PC), sphingomyelin, and galactosyl ceramide, while negative mode is used to detect phosphatidylethanolamine (PE)[12].

Another direct-infusion method, based on electrospray ionization tandem mass spectrometry (ESI-MS/MS), was described by Brügger and coworkers in 1997. This method, which utilizes a triple-quadrupole mass spectrometer, was a breakthrough for lipidomics research because it allowed for the full identification and quantitation of compounds within a crude lipid extract with moderate experimental complexity, high sensitivity, and reproducible results[13]. A triple-quadrupole mass spectrometer has three quadrupoles; Q_1 and Q_3 function as mass analyzers, while Q_2 serves as a collision cell. Inside the mass analyzers, ions are in an electric field and, at a given voltage, a specific mass-to-charge (*m/z*) ratio moves straight at the detector. For most lipids, the charge is 1, so *m/z* is typically equal to the mass of the ion. Ion polarity is chosen in the source, which allows for the selection of lipid classes based on their propensity to form positive $[M+H]^+$, negative $[M-H]^-$, or other ions. When only one mass analyzer is used (ESI-MS), lipid molecular species are detected within the range of masses scanned on the mass analyzer in either positive $[M+H]^+$ or negative $[M-H]^-$ mode. The use of ESI-MS results in a small number of complex spectra. One disadvantage of ESI-MS (with a single-quadrupole MS) is that signals from compounds with the same *m/z* overlap, which makes the spectra difficult to interpret. On the other hand, ESI-MS/MS provides a series of easy to read spectra for individual lipid classes, which allows the resolution and quantification of isobaric species without additional product analyses. The Brügger et al. ESI-MS/MS method exploits the fact that a

common fragment is formed by lipids within the same class after collision induced dissociation by utilizing precursor ion and neutral loss scans[12].

In tandem mass spectrometry (ESI-MS/MS), Q1 and Q3 are mass analyzers and Q_2 is the collision cell. For a precursor ion scan, also known as a parent ion scan, Q3 is set to allow only a fragment ion of one *m/z* ratio to pass, while Q1 sequentially scans for all molecular species that created that product ion in the collision cell and spectra are presented as a function of Q1 *m/z*. For a neutral loss scan, both Q_1 and Q_3 are scanned together and Q_3 is offset by the neutral loss of interest and, again, spectra are presented as a function of Q1 *m/z*. For a product ion scan, also known as a daughter ion scan, Q_1 is set to allow the transmission of only one *m/z*, and Q_3 sequentially scans for all fragments created by compounds with that *m/z* in the collision cell and spectra are presented as a function of Q3 *m/z*[13]. A precursor ion scan provides information about the molecular species within classes of lipids that have a charged common fragment, whereas a neutral loss scan provides the same information for classes of lipid that have an uncharged common fragment. For a complete lipid profile, a series of precursor ion and neutral loss scans are acquired sequentially while the sample is continuously infused, using an autosampler [13]. For information about specific acyl groups, such as the number of carbons and the number of double bonds, product ion analysis can be applied to reveal the nature of the fatty acid components in each lipid molecular species. However, this is not always necessary because many lipid species consist of only one combination of fatty acids present in the organism from which they are derived[14].

For ESI-MS based techniques, quantification of lipid molecular species is less complicated, requiring fewer internal standards than ESI-MS/MS methods because the signal from each scan are directly proportional to the amount of each lipid. For tandem mass spectrometry, signal intensity is dependent on both mass and the energy used for fragmentation, thus, the response of the instrument as a function of mass is required [12]. Using ESI-MS/MS, quantification of resolved lipid molecular species is achieved using an internal standard containing two lipids in each head-group class, which is mixed with individual samples and simultaneously infused. The internal standard is a cocktail of lipids, containing fatty acyl constituents that are not found in nature to ensure signal from the standard does not overlap with signal from the sample. A known molar amount of each internal standard is added to each sample analyzed, and quantification is achieved by generating a standard curve that correlates the known molar amount of internal standard to signal for each lipid class [13]. This quantification method is sensitive to the sub-picomolar level, and, combined with genetic manipulations and other treatments, can be used to investigate correlations between quantitative changes in lipid molecular species and genetic manipulations or treatments. This "lipidomic" approach is a powerful tool for investigating the molecular mechanisms underlying lipid metabolism and regulation in biological systems.

The Brügger et al. method opened the door for sensitive high-throughput profiling of crude lipid extracts from yeast and animals. Plant lipids, on the other hand, presented a new challenge due to the presence of lipid molecular species such as monogalactocyldiacylglycerol (MGDG), digalactosyldiacylglycerol (DGDG), and sulfoquinovosyldiacylglycerol (SQDG) which are unique to the chloroplast [12]. Welti and colleagues devised a method for the comprehensive analysis of chloroplast lipids in the presence of bulk plant polar lipids[15,16]. This expansion of the

Brügger et al. method is quick and simple, involving the separation of plant lipid extracts into two aliquots for mass spectral analysis. Because the galactoglycerolipids MGDG and DGDG are uncharged species, they were analyzed in the presence of sodium acetate with precursor scans for positively charged sodium adducts of *m/z* 243. SQDG, on the other hand, is negatively charged at a neutral pH and was analyzed from the second aliquot in the presence of ammonium acetate using scans described by Brügger[16].

.

The unfortunate drawback of shotgun experiments, such as ESI-MS, which do not separate classes of lipids using chromatography prior to analysis are mass ambiguities resulting from signal overlap. The cellular lipidome is a complex mixture which comprises some isobaric species that cannot be distinguished by conventional low resolution mass spectrometry[17]. In mass spectrometry, the detected ion signal (voltage, current, time-of-flight, etc.) is digitized and the resolving power, or the ability of an instrument to distinguish two different peaks/signals, depends on the mass analyzer used[18]. As mass resolving power increases, new chemical information becomes accessible. An alternative approach to shotgun lipidomics involves the use of high resolution mass analyzers, such as time-of-flight (TOF) and Fourier transform mass analyzers, which provide separation of nominally isobaric species[19]. Progress in high resolution mass spectrometry has changed the concept of lipidome characterization by streamlining and simplifying the process[17].

Improvements in our ability to profile complex lipids by mass spectrometry and expansion of these techniques to include plant lipids paved the way for functional studies which examine the role lipid changes play in plant biological processes. These methods, combined with reverse-

genetics and other genomics approaches, such as genome wide association study (GWAS), are being employed to identify genes and proteins involved in lipid metabolism and to examine associations between genetic variation, lipid composition, and plant growth, development, and stress signaling responses. This strategy has been utilized to identify lipid metabolic pathways involved in stress response, elucidate the roles of specific genes and enzymes, and to identify the lipid substrates and products of certain enzymes, including lipid-metabolizing proteins which play a role in plant defense responses[12]. In one such study, Welti et al. (2002) analyzed lipid extracts of leaves from the model plant *Arabidopsis thaliana* under cold acclimation and freezing conditions using ESI-MS/MS. The analysis revealed significant changes in membrane composition associated with response to temperature stress, and pinpointed a few of the major metabolites involved. The results showed a noteworthy increase in phosphatidic acid (PA), with corresponding decreases in other phospholipid species including phosphatidylethanolamine (PE), phosphatidylglycerol (PG), and phosphatidylcholine (PC), suggesting the activation of phospholipase D (PLD) which is known to hydrolyze phospholipids from the membrane yielding PA. Furthermore, increases in lysophospholipids, including lysoPC and lysoPE suggested phospholipase A activation. To investigate the role of PLD and its products in response to temperature stress, lipid profiles of wild type *Arabidopsis* and plants deficient in PLDα_1 that had been exposed to freezing were compared. PLDα_1 deficiency led to a ~50% decrease in the amount of PA formed during freezing and, interestingly, resulted in increased resistance to freezing. Moreover, while *in vitro* PLDα_1 is known to act on PC, PE, and PG, only the decrease in PC was significantly affected in PLDα_1-deficient plants, suggesting PC is the main substrate for PLDα_1 *in vivo* [15]. Studies such as this, which aim to identify key enzymes and metabolites

involved in freezing response, have led to great advances in our understanding the role of lipids in plant cold and freezing tolerance.

This strategy can also be applied to identify lipid-associated genes and proteins which play a role in other cellular processes, such as defense signaling. To identify lipid-metabolizing enzymes related to plant defense signaling, Shah and colleagues utilized a mutation in an *Arabidopsis* stearoyl acyl carrier protein desaturase, *suppressor of salicylic-acid insensitivity2 (ssi2)* or *fatty-acid biosynthesis2 (fab2)*, which causes constitutive salicylic acid signaling[20]. Random mutagenesis of *ssi*2 seeds resulted in the identification of four different suppressor genes. Two of which, *sfd4* (an allele of *FATTY ACID DESATURASE 6* (*FAD6*)), and *sfd1* (an allele of a gene encoding a dihydroxyacetone phosphate reductase), showed reduced levels of galactolipid species assembled in the plastid, pointing to a role for plastidic lipid metabolism in defense signaling[20] . In a more recent study, Li and colleagues identified an Arabidopsis mutant, *ar21,* which has a novel seed fatty-acid phenotype characterized by higher levels of eicosanoic acid (20:1) and oleic acid (18:1) and a reduced level of α-linolenic acid (18:3)[21] . They used a combination of map-based cloning and whole genome sequencing to identify the mutation associated with this phenotype as a lesion in the plant-specific eukaryotic translation initiation factor eIFiso4G1. Genetic analysis on developing seeds showed reduced expression of plastid encoded genes. Specifically, decreases in both transcript and protein levels of an enzyme involved in fatty acid biosynthesis, the b-subunit of the plastidic heteromeric acetyl-CoA carboxylase (htACCase) were observed[21]. Through studies such as this, we have gained considerable insight into the activities of suppressor gene substrates/products and possible roles of transcription factors, lipid molecular species, and lipid-derived signals.

Plant Membrane Lipid Biosynthesis

The leaves of higher plants utilize two distinct pathways for galactoglycerolipid synthesis, the eukaryotic pathway (endoplasmic reticulum) and the prokaryotic pathway (chloroplast). Membrane biogenesis in higher plants involves the flux of fatty acids and lipids between these two organelles, each containing a unique set of enzymes which influences the lipid molecular species resulting from assembly therein. Lipid biosynthesis begins with fatty-acid synthesis in the chloroplast by fatty acid synthase (FAS II), which is an enzyme complex composed of multiple dissociable enzymes and a central acyl carrier protein (ACP). This enzyme complex synthesizes fatty acids starting with acetyl-CoA and malonyl-ACP by progressively extending the carbon chain adding two carbons at a time. This involves a condensation reaction producing a 3-oxoacyl-ACP, catalyzed by 3-oxoacyl-ACP synthases (KAS), and the subsequent reduction of the 3-oxo group by a 3-oxoacyl-ACP reductase, a 3-hydroxyacyl-ACP dehydratase, and an enoyl-ACP reductase[22]. Each extension cycle produces a saturated acyl-ACP, which is the substrate for condensation with malonyl-ACP in the next cycle. After fatty-acid biosynthesis, 18:0 fatty-acids are desaturated to 18:1 by FATTY ACID BIOSYNTHESIS2 (FAB2) in the plastid[23], and acyl-ACPs (mostly $C_{16:0}$ and $C_{18:1}$), are finally hydrolyzed by acyl-ACP thioesterase. According to the two-pathway model, these 16:0 and 18:1 fatty acids either stay in the chloroplast envelope for production of chloroplast lipids or they are transported to become CoA esters in the cytosol/endoplasmic reticulum (ER). Lipid exchange between the chloroplast and ER is bidirectional, and several Arabidopsis mutants affected in the flux of lipids between the ER and chloroplast have been described. Multiple transport proteins have been identified, including *TRIGALACTOSYLDIACYLGLYCEROL (TGD)* proteins TGD 1-4, which have been shown to be associated with lipid transfer from the ER to the chloroplast[24].

The products of fatty-acid synthesis bound for the prokaryotic pathway, 16:0 and 18:1, are esterified to the *sn*1 and *sn*2 positions of glycerol-3-phosphate by the enzymes ACYL TRANSFERASE1 (ACT1) and ACYL TRANSFERASE2 (ACT2), respectively[2]. Lysophosphatidic acid (LPA), produced by ACT1, is converted to phosphatidic acid (PA(18:1/16:0)) by ACT2 then either converted to phosphatidylglycerol (PG), or to digalactosyldiacylglycerol (DAG) for making galactoglycerolipids or sulfolipids. All lipids resulting from assembly via the prokaryotic pathway (in the chloroplast) contain 18:1 at the sn1 position, and 16:0 at the sn2 position when they are initially synthesized[25]. The 16-carbon fatty acid at the sn2 position of these lipids can be desaturated in two different ways depending on the lipid class. Generally, ~30-70% of the 16:0 on PG is converted to Δ3-*trans*-16:1 by FAD4 and ~30-70% remains 16:0 (Figure 1.1). For galactoglycerolipids, 16:0 at the sn2 position of MGDG is desaturated to *ω*9-*cis*-16:1 by FAD5, which is then desaturated to 16:2 by FAD6, and finally to 16:3 by FAD7 or FAD8. 18:1 attached to the sn1 position is converted to 18:2 and 18:3 by FAD6 and FAD7 or FAD8, resulting in membrane galactoglycerolipids with one 16-carbon fatty acid with three double bonds and one 18-carbon fatty acid with three double bonds (18:3/16:3) (Figure 1.1)[25].

The traditional view is that fatty-acids bound for the eukaryotic pathway, mostly 18:1 fatty acids, are converted to CoA esters, while being transported to the ER where they are attached to glycerol-3-phosphate to make lysophosphatidic acid (LPA) by glycerol-3-phosphate acyltransferases (GPATs). LPA is acylated to form phosphatidic acid PA (18:1/18:1) or PA(16:0/18:1). The PA produced is subsequently dephosphorylated to diacylglycerol

(DAG(18:1/18:1) or DAG(16:0/18:1)), then converted to phosphatidylcholine (PC(18:1/18:1) or PC(16:0/18:1)(Figure 1.1)[25]. However, metabolic labeling experiments revealed the majority of newly synthesized FAs actually enter PC directly through a process termed "acyl editing", a deacylation-reacylation cycle which exchanges FAs on PC with FAs in the acyl-CoA pool through the acylation of lysophosphatidylcholine (LPC) by acyl-CoA lysophosphatidylcholine acyltransferases (LPCATs) [26, 27, 28, 29]. In the ER, FAD2 desaturates 18:1 attached to both positions to 18:2, then PC(18:2/18:2) either stays in the ER and is desaturated to PC(18:3/18:3) by FAD3, or it is transported back to the chloroplast where it is used to make membrane glycerolipids MGDG, DGDG, or SQDG and the FAs attached are desaturated to (18:3/18:3) by FADs 7/8 (Figure 1.1). The eukaryotic pathway chiefly produces membrane galactoglycerolipids with two 18-carbon fatty acids and three double bonds (18:3/18:3), although it does produce some galactoglycerolipids with 16:0 at the *sn*1 position (mainly found in DGDG) [25].

Although two discrete galactoglycerolipid assembly pathways exist, the physical advantages and disadvantages of synthesis of chloroplast lipids through one pathway or the other have yet to be characterized. Interestingly, not all plants use both pathways for galactoglycerolipid assembly. Some plants, termed "16:3 plants", use both routes, resulting in thylakoid membranes made up of both (18:3/16:3) and (18:3/18:3) glycerolipids, whereas others, termed "18:3 plants", only utilize the endoplasmic reticulum route, resulting in thylakoid membranes made up largely of (18:3/18:3) galactoglycerolipids. Presumably, 18:3 plants lost the ability to utilize the chloroplast for galactoglycerolipid assembly at some point in evolutionary history. Data from a screen of over 400 different plant species suggested primitive plants had both pathways. The prokaryotic pathway has been lost independently over the evolution of many different plant species, and

scientists have yet to discover why[30]. On the other hand, many plants in different families have maintained the prokaryotic pathway. Surprisingly, there does not seem to be a link between the presence/absence of the prokaryotic pathway and environmental factors or the general anatomy of the plant species[31].

Fatty Acid Desaturation in Plants

Fatty acid desaturation is the enzymatic removal of 2 hydrogens from methylene groups on an acyl chain, creating a carbon-carbon double bond[32]. Fatty acids in the lipids of photosynthetic organisms are often further desaturated, forming polyunsaturated fatty acids with levels that vary with growth temperature and other environmental conditions. In general, the lower the growth temperature the higher the degree of unsaturation (i.e., the more polyunsaturation). The functional significance of the high proportion of unsaturated fatty acids in plants and other photosynthetic organisms has been investigated through the characterization of several mutants of Arabidopsis deficient in various desaturases, which differ in substrate specificity, subcellular localization, and/or mode of regulation. These mutants, identified by analyzing leaf lipids of heavily mutagenized plants, disrupted the activities of fatty acid desaturases termed FAB2 and FAD2, 3, 4, 5, 6, 7, and 8 (Table 1.1). All genes identified were confirmed by using cloned genes to complement mutations in transgenic Arabidopsis[33]. ER- and plastid-localized fatty acid desaturases act on different lipid molecular species, and utilize different intermediate electron donors. The addition of a double bond, which converts most of newly synthesized stearic acid to oleic acid is added by the soluble enzyme, FAB2 (stearoyl ACP desaturase) in the chloroplast[33]. ER-localized enzymes typically act on fatty acids esterified to PC and utilize cytochrome b_5 as an electron donor, whereas chloroplast-localized enzymes typically act on fatty acids esterified to

galactoglycerolipids, SQDG, and PG and use soluble ferredoxin as an electron donor. Soluble desaturases, such as the stearoyl-ACP desaturases, do not show significant homology to membrane-bound desaturases. Despite the differences in substrate specificity, electron donors, and the position of the double bond produced, all membrane bound fatty acid desaturases described to date are structurally related and share common structural motifs with hydroxylases and epoxidases[33].

Two electrons are needed for the formation of one double bond, and functionally equivalent electron transport systems in the plastid and ER supply these electrons in the form of the reducing equivalents NADPH or NADH, respectively. In a desaturation reaction, pairs of electrons from these reducing equivalents are simultaneously transferred to a flavoprotein, which sequentially releases the electrons to two carrier proteins capable of carrying only one electron at a time. The carrier proteins transfer electrons to the desaturase resulting in the two-electron reduction and introduction of a double bond. The reducing equivalents required for this reaction depend on the subcellular localization of the desaturase, not whether it is soluble or membrane bound. For chloroplast-localized desaturases, the reaction mechanism depends further on the type of tissue in which it resides. In non-photosynthetic tissues and in the dark, NADPH is used with ferredoxin-$NADP^+$ oxidoreductase and the electron carrier is 2Fe-2S ferredoxin. In photosynthetic tissues, on the other hand, the reducing equivalents from photosystem I are directly transferred to ferredoxin which supplies the desaturase independently of ferredoxin-$NADP^+$ oxidoreductase. For ER-localized desaturases, reducing equivalents are supplied by NADH to cytochrome b_5 reductase, and the electron carrier is cytochrome b_5. One notable

distinction between these two systems is the difference in electrochemical potentials between the two electron carriers [E°s of -420 mV for ferredoxin and -24 mV for cytochrome b5][32].

Much of what we know about the molecular catalysis of soluble desaturases came from analysis of the crystal structure of the Δ^9-18:0-ACP desaturase from castor (Figure 1.2). The soluble desaturase is a homodimer [34], and the secondary structure of the monomer is primarily α-helical, except a small C-terminal β-hairpin. The monomer has 11 total α-helices with 2 capping each end, 9 forming a core bundle, and 4 of those 9 coordinating the diiron cluster at the active site buried in the middle of the structure. This crystal structure confirmed the histidine ligands proposed by sequence alignments, as well as revealing previously unidentified glutamic acid ligands which participate in coordination of the diiron cluster[35] . It also revealed a hydrophobic channel extending from the surface to the deep interior of each subunit which likely represents the substrate binding pocket, as it would position the fatty-acid substrate in proximity to the active site diiron cluster. The discovery of this hydrophobic pocket provided insight into the substrate and regiospecificities of soluble acyl-ACP desaturases, indicating an acyl chain modeled into the pocket would assume a bent conformation at the Δ^9 carbon within catalytic distance from the active site diiron cluster. The size of this hydrophobic pocket is large enough to accommodate acyl chains with 18-carbons or less, consistent with the substrate specificity of the Δ^9-18:0-ACP desaturase, although surface interactions between ACP and the desaturase and residues lining the hydrophobic channel may also influence substrate specificity[33,35].

Our understanding of membrane bound desaturases has lagged compared to that of soluble desaturases, largely due to technical challenges associated with obtaining large amounts of

purified membrane proteins and with their crystallization[32]. Genetic approaches have proved superior to biochemical approaches for the study of these enzymes. Gene sequencing, cDNA sequencing, and heterologous probing has resulted in the isolation of a large family of desaturase genes from various organisms, including Arabidopsis. While structural analysis and direct investigation of these enzymes has lagged compared to soluble desaturases, an abundance of sequence data has been collected[33]. Analysis of the deduced amino acid sequences of several membrane-bound desaturases revealed the iron binding motif found in soluble desaturases [(D/E) $X_2H]_2$ is not conserved in integral membrane desaturases[36]. Instead, all membrane-localized desaturases from plants and other organisms contain a pair of histidine-rich sequences, called histidine boxes (HXXHH), which make up the proposed active site, and are in equivalent positions in relation to predicted membrane-spanning domains. The histidine boxes are believed to coordinate the diiron cluster because they are critical to desaturase function and are located on the cytoplasmic face of the membrane[33,37,38]. Integral membrane desaturases have evolved at least three distinct methods of positioning double bonds. Several desaturases have been shown to count carbons from the carboxyl end of the acyl-chain in a fashion similar that of the soluble ACP-desaturase previously described[39]. In contrast, some desaturases count from the methyl end of the acyl chain and a third class of desaturases, the $\omega 6$ desaturases, count toward the methyl end from an existing double bond in the monoene which is used as a reference point[33,40].

Understanding the molecular mechanisms of integral membrane proteins requires the elucidation of their structures to high resolution. The structural characterization of membrane bound fatty acid desaturases is possible using three general methods: electron microscopy, nuclear magnetic resonance (NMR), and x-ray crystallography. Unfortunately, most membrane proteins exist in

complexes too large to be analyzed using NMR and the hydrophobic surfaces and anisotropic orientation of integral membrane proteins present serious challenges for producing well-ordered three-dimensional crystals using traditional approaches. One critical element, which is unique to the crystallization of membrane proteins, is the successful removal of the protein from its native bilayer by solublization using detergents. This creates complications with crystallization because most integral membrane proteins are vulnerable when solubilized and slight perturbations in their structure can lead to denaturation, aggregation, and even degradation by proteases. Upon reconstitution, the proteins often regain stability suggesting the release of lateral pressure from the membrane could be the cause of problematic structural perturbations. In 1996, Landau and Rosenbusch devised an approach, based on this idea, designed to keep membrane proteins in a quasisolid membrane environment throughout the crystallization process. This utilizes a membrane system method, termed lipidic cubic phase, consisting of lipid, water, and protein in appropriate ratios to create a complex three-dimensional lipidic array[41]. In 2015, Bai and colleagues used this technique to determine the crystal structure of a mammalian stearoyl-CoA desaturase (SCD1) bound to its substrate, stearoyl-CoA, at 2.6 Å resolution (Figure 1.3). SCD1 is an ER localized integral membrane protein which catalyzes the formation of a *cis*-double bond between carbons 9 and 10 of stearoyl-or palmitoyl-CoA and utilizes cytochrome b_5 as an electron donor. The protein has four transmembrane helices (TM1-4) arranged in a cone-like shape with TM4 in the center of the cone positioned between TM1 and TM2. The cone is capped by a cytosolic domain containing a substantial non-protein density consistent with an 18-carbon CoA molecule and modeling a stearoyl-CoA molecule into this density it appeared to interact primarily with conserved hydrophilic and charged residues on the outer surface of the cytosolic domain. These residues are conserved among known stearoyl-CoA desaturases but not stearoyl-

lipid desaturases, suggesting they are important for determining the substrate specificity of the enzyme[42].

The functional characterization of integral membrane fatty acid desaturases is typically achieved through cloning and heterologous expression in yeast (*Saccharomyces cerevisiae).* For example, Lee and colleagues identified four perilla fatty acid desaturase genes (*Pfr*FAD2-1, *Pfr*FAD2-2, *Pfr*FAD3-2, and *Pfr*FAD7-2) using random amplification of complementary DNA ends and sequence data obtained using RNA-seq. To characterize these genes, they first looked at expression and localization using quantitative real-time polymerase chain reaction (qRT-PCR) and by transforming *Arabidopsis* protoplasts with perilla genes fused to green fluorescent protein. Then, to confirm the proposed activities of the fatty acid desaturase genes, they were cloned and transformed into yeast. The results showed the perilla fatty acid desaturase genes were functional in budding yeast and confirmed their proposed function, indicated by the presence of 18:2 in yeast expressing *Pfr*FAD2 and the presence of 18:3 in yeast expressing the ω3 fatty acid desaturase gene[43].

In addition to confirming the proposed functions of desaturase genes, yeast expression can be used to investigate the substrate specificity and molecular mechanisms of the proteins they encode. For example, Hoffmann and colleagues used this technique to compare the substrate specificities of two integral-membrane desaturases from *Aspergillus nidulans*, one a monofunctional oleoyl-Δ12 desaturase and the other a processive bifunctional oleoyl-Δ12/linoleoyl-ω3 desaturase (An2 and An1, respectively). The two desaturase genes were identified by searching the *A. nidulans* genome for sequences highly similar to known desaturase

sequences from plants. Genomic sequence information was used to design primers to amplify cDNAs of the putative desaturases and the substrate specificities were confirmed by cloning the open reading frames of both cDNAs into yeast. The results provided some insight into substrate specificity, indicating the oleoyl-Δ12 desaturase (A2) preferred 18-carbon fatty acids when compared to 16-carbon fatty acids, and that the processive bifunctional enzyme (A1) preferentially converts 18-carbon fatty acids to ω3-fatty acids followed in preference by 20-carbon fatty acids. Furthermore, the introduction of the second double bond (ω3 position) of the bifunctional enzyme is catalyzed more efficiently than the first (Δ12 position). The high sequence similarities of the primary sequences of A2 and A1 provided an ideal framework for investigating factors influencing substrate specificity and bifunctionality. The two desaturases were divided into nine domains based on topology models, and the domains of the monofunctional enzyme were systematically exchanged for the corresponding matches of the bifunctional sister enzyme. The hybrid enzymes were heterologously expressed in yeast and catalytic capacities were measured by analyzing and comparing the resulting fatty acid patterns. The exchange of two specific domains of a length of 18 or 49 amino acids each was sufficient to convert the monofunctional parental enzyme to a processive bifunctional $\Delta 12/\omega 3$ desaturase, indicating substrate specificity and bifuntionality could be narrowed down to a membrane peripheral region close to the active site[44].

Biological Roles of Polyunsaturation

Lipid desaturation is particularly important in plants, and other heterothermic organisms, because they must adapt to ambient temperature, which fluctuates over relatively wide limits. This presents a challenge because membrane lipid fluidity must be maintained within a certain range

to preserve membrane function. Membrane fluidity is imperative for the function of trans-membrane and membrane-associated proteins, the diffusion of lipids and proteins within the membrane, membrane biogenesis during cell division, and more. The fluidity of a biological membrane at a given temperature depends primarily on lipid composition and, more specifically, on the nature of the hydrocarbon tails attached to the lipid head group. Membranes tend to become less fluid as temperatures decrease; in response, lipid molecular species with shorter hydrocarbon tails and an increasing degree of unsaturation can be formed or incorporated to increase membrane fluidity. If fluidity is not maintained or environmental conditions exceed normal limits, biological membranes may undergo gross structural changes driven by phase changes in membrane lipids, resulting in loss of selective permeability, disruption of cellular transport processes[45].

Freezing and cold tolerance are critical factors in determining the geographic range in which wild plant species are distributed and agricultural crops can be cultivated. Freezing damage in transitional climate zones can have a devastating effect on agriculture, which is of substantial concern due to growing challenges in food production associated with global climate change and feeding a growing population. Freezing causes extracellular ice formation which results in decreased water potential across the plasma membrane and leads to severe cellular dehydration. Furthermore, formation of non-bilayer structures can lead to leakiness of biomembranes enclosing the cell, or organelles within. To minimize membrane damage from cold and freezing conditions, plants may undergo a process called cold acclimation during which membrane lipid composition is altered by increasing fatty acid desaturation, amongst other lipid modifications, many of which are associated with increased freezing tolerance[46]. The advantage of having an

increased level of desaturation in biological membranes during cold and freezing conditions is evident when it is considered, for example, that the introduction of a single double bond decreases the melting temperature of stearic acid (18:0), a major fatty-acid attached to membrane phospholipids, by up to 56℃. The addition of a double bond also changes the molecular shape of the lipid, which in turn influences bilayer packing and membrane behavior[47]. In addition to being associated with cold acclimation and freezing tolerance, fatty acid desaturation has been shown to impact chloroplast development and photosynthetic efficiency. Phenotypic analysis of plants with mutations in fatty acid desaturase-encoding genes display differences in chloroplast morphology, membrane biogenesis, and recovery from low temperature-induced photoinhibition between mutant and wild type plants[47,48]. In one study, Suzanne Hugly and Chris Somerville analyzed Arabidopsis plants with mutations in four putative fatty acid desaturases (*FAD*4, *FAD*5, *FAD*6, *FAD*7), each showing significant changes in chloroplast fatty acid composition. Interestingly, the plants showed no obvious visible phenotype under normal growth conditions (100-150 μmol m^{-2} s^{-1} PAR, 22℃), but, analysis of leaves using electron microscopy (EM) revealed alterations in chloroplast organization and ultrastructure in several mutant lines, inferring a role for polyunsaturated lipids in chloroplast development and/or structural maintenance. Moreover, developing leaves of two mutant lines (*FAD*5 and *FAD*6) became chlorotic when grown at temperatures below 5℃. Analysis of electron micrographs from those mutants revealed dramatic changes in chloroplast size, membrane content, and structural organization. Similar effects were not seen in fully developed leaves after transferring plants to low temperature, suggesting the observed morphological changes are related to impaired chloroplast development rather than a reduction in membrane stability[48].

Low temperature-induced photoinhibitory damage is a major cause of plant chilling sensitivity, and thylakoid fatty acid composition, specifically, appears to have a large influence on photoinhibition in higher plants. Thylakoids are flattened sacks bounded by pigmented membranes in the chloroplast which house the light harvesting and electron transport reactions of photosynthesis. Thylakoid membranes have a unique and characteristic lipid composition, primarily containing highly unsaturated trienoic fatty acids (18:3 and 16:3) which, in Arabidopsis, make up about two thirds of the fatty acids within the membrane, and over 90% of the fatty acids attached to the most abundant thylakoid lipid, MGDG[49]. A major mechanism of photoinhibition occurs through inactivation of the D1 protein of photosystem II due to damage, directly proportional to light intensity, from the sun or another light source. For recovery from photoinhibition, the inactivated D1 proteins must be replaced by newly synthesized proteins. The overall extent of photoinhibition *in vivo* is believed to depend on the balance between inactivation and recovery[49]. In a 1997 study, Kanervo et al. found the rate of recovery from photoinhibition was directly related to thylakoid lipid composition in cyanobacteria grown at low temperatures. Mutant cyanobacteria lacking all polyunsaturated fatty acids were significantly more susceptible to photoinhibitory damage, and expression of a Δ12-desaturase (*Des*A) on the mutant background was shown to increase the low-temperature tolerance of photosystem II[50]. Work on a mutant of Arabidopsis, *fad*3-2 *fad*7-2 *fad*8, deficient in three fatty acid desaturases, demonstrated a similar phenomenon in higher plants[49].

The effects resulting from disruptions in fatty acid desaturation are not limited to membranes and reactions that occur within membranes. The products of fatty acid desaturation may serve as important signaling molecules or precursors to signaling molecules, such as prostaglandins and

pheromones in animals, or oxylipins in plants, involved in growth, development, and/or defense response pathways. For example, Mei and colleagues conducted an experiment in which cell suspension cultures using three different types of plant cells: *Acer pseudoplatanus* (Sycamore maple), leaf meristem cells of *Arabidopsis thaliana*, and callus cultures of meristem cells of Arabidopsis were grown and analyzed for a possible correlation between growth rate and variations in FA unsaturation[51]. While no significant changes were observed for 16-carbon species, the level of unsaturation of 18-carbon species varied significantly between fast and slow growing cultures. During exponential phase, both 18:3 and 18:2 decreased with a corresponding increase in 18:1, indicating the rate of desaturation of 18:1 decreased during the fast-growing stage[51]. Furthermore, trienoic fatty acids are known to serve as precursors of plant hormones, such as jasmonates which are involved in defense signaling, wound response, development, and adaptation to environmental conditions/stresses. Increased expression of *FAD7* (which encodes an enzyme that desaturates 18:2 to 18:3 in the plastid) has been observed in a wound-responsive pattern, consistent with increased demand of trienoic fatty acids for jasmonic acid synthesis[52]. Disruptions in JA signaling have a dramatic effect on important plant physiological processes including defense gene expression, growth/development, and fertility[53].

FAD6 and *ω*6 desaturation

Fatty acid desaturase 6, or *FAD6*, is a chloroplast localized *ω*6-fatty acid desaturase which catalyzes the introduction of a double bond in the biosynthesis of 16:3 and 18:3 fatty acids in the chloroplast (Figure 1.1 and Table 1.1). It is an integral-membrane protein 418 residues and ~48,000D which resides in the chloroplast inner membrane and uses soluble ferredoxin as an electron donor. *FAD6* acts on 18:1 and 16:1 fatty acids, with a previously existing double bond at

ω9, esterified to the *sn*1 or *sn*2 positions of galactoglycerolipids, SQDG, and PG in the chloroplast. The first mutant of *Arabidopsis fad6* (*fad6*-1) was identified and biochemically characterized by Browse and colleagues in 1989. This mutant was isolated by screening an M2 population of plants following mutagenesis with ethyl methane sulfonate (EMS) for alterations in fatty-acids extracted from leaf samples using gas-liquid chromatography (GLC) analysis[54]. Biochemical analysis of this mutant revealed a significant increase in 18:1Δ9 and 16:1Δ7 fatty-acids with corresponding decreases in 18:2(Δ9,12), 16:2(Δ7,10), 18:3 (Δ9,12,15), and 16:3 (Δ7,10,13). While 18:3 fatty-acids showed a substantial decrease in mutant vs. wild type plants, 16:3 fatty-acids were virtually absent in the mutant. Since MGDG assembled in the chloroplast is the substrate for 16:3 synthesis, it was concluded that the desaturase is localized to the chloroplast and the 18:2 and 18:3 present in the mutant were likely desaturated in the endoplasmic reticulum[54].

In *Arabidopsis* and other 16:3 plants, MGDG contains 16:3 only at the *sn*2 position of the glycerol backbone; chloroplast assembled PG however, contains 18:3 mainly at the *sn*1 position. The *fad6* mutant identified by Browse and colleagues showed significant decreases in both 16:3 in MGDG and 18:3 in PG, indicating the enzyme is not specific to the position on the glycerol backbone, length of the acyl chain, or lipid head group[54]. Furthermore, when 16:0 is present at the *sn*2 position of PG, *sn*1 position of DGDG, or either position of SQDG it is not desaturated, indicating the desaturase requires a previously existing double bond at the ω9 position. The fact that 18:1 and 16:1 accumulated in the mutant instead of the Δ9,15-isomer of 18:2 and the Δ7,13-isomer of 16:2 suggested the ω3 desaturase in the chloroplast (*FAD*7) requires the presence of a double bond at the ω6 position[54]. Moreover, since *FAD*6 resides in the chloroplast it would be

expected only galactoglycerolipids, PG, and SQDG would be affected. However, phospholipids derived from the endoplasmic reticulum (PC, PE, and PI) also showed a twofold increase in 18:1 compared with wild type, suggesting both chloroplast and extrachloroplast desaturases influence the level of desaturation of phospholipids in extrachloroplastidic membranes[54]. It was also noted that the heterozygous F1 progeny of a cross between the wild type and *fad6* mutant line had higher levels of 18:1 and 16:1 fatty-acids than wild type, indicating the wild type allele is incompletely dominant. Furthermore, the mutant was slightly lighter than wild type under normal growth conditions but was otherwise healthy and vigorous[54].

Although the first mutant of *Arabidopsis fad6* was identified and biochemically characterized in 1989, the gene was not identified until 1994 when Somerville et al. reported the isolation and characterization of a cDNA clone encoding the ω6 desaturase[55]. A mixed oligonucleotide was designed based on analysis of amino acid sequences of the *Brassica* ω3 desaturase (*fad3)*, the cyanobacterial Δ12 desaturase (*desA*), and *Arabidopsis* ω3 desaturases (*fad7* and *fad8*). The sequence GHDCGH was found to be conserved in all four sequences, therefore a 17-bp, 128-fold degenerate oligonucleotide encoding the conserved sequence was used to probe an *Arabidopsis* cDNA library [55]. One clone identified in the screen exhibited high sequence similarity to the cyanobacterial Δ12 desaturase (*desA*), so the *des*A sequence was used to re-screen the library for a full-length clone. The isolate with the longest cDNA insert genetically mapped to the same location as the *fad6* mutant, and complemented the *fad6* mutation in transgenic *Arabidopsis*[55]. Analysis of the nucleotide sequence of this insert revealed a 1.2kb open reading frame encoding a 418-amino acid polypeptide with a predicted molecular mass of ~48 kD. Comparing the deduced amino acid sequence to that of the cyanobacterial Δ12 desaturase (*desA*) revealed the

sequences are 54% identical and 71% similar. In contrast, comparing the *fad6* sequence to that of the ER localized ω6 desaturase (*fad2*) from *Arabidopsis* revealed a surprisingly low level of homology (24% identical and 49% similar). This is in stark contrast to ω3 desaturases, which show a high level of homology, ranging from 55 to 84%, even between different plant species [55]. The cDNA probe was also used to analyze expression of the gene at a transcriptional level using mRNA extracted from leaves of wild type and *fad6-1* mutant plants at different developmental stages. No significant difference in *fad6* expression was observed in mutant vs. wild type, suggesting no mechanism exists to sense the level of polyunsaturation of chloroplast membranes and alter the expression of the *fad6* gene to compensate for the mutation. Additionally, a progressive decline in *fad6* mRNA during the later stages of growth was observed in both mutant and wild type, presumably reflecting the decreased demand for membrane lipids in fully expanded vs. expanding leaves[55].

The *fad6-1* mutation was finally sequenced by Zheng and colleagues in 2009; these workers sought to dissect the possible function of the *FAD6* gene in different stress conditions. To achieve this goal, they isolated the mutant allele of the gene (*fad6-1*) from the Arabidopsis Biological Resource Centre (CS207)[56]. Sequence analysis indicated the mutant line harbored a single base change on the fourth exon 954 bp downstream of the ATG start codon. This G to A transition causes an amino acid change (Gly_{160}→Arg) in one of the predicted transmembrane domains of the desaturase[56]. To investigate possible biological functions of the enzyme, the researchers examined expression patterns of the *FAD6* gene under normal conditions as well as different stress conditions by RT-PCR and qRT-PCR. They found that *FAD6* was expressed in seedlings as well as several tissues including roots, rosette leaves, stems, flowers, and siliques.

The transcript levels of *fad6* seedlings exposed to various abiotic stresses indicated stress signals including salt and mannitol significantly induced expression of the gene[56]. When the root growth of mutant and wild type seedlings were examined in seedlings grown under high salt stress conditions, the results showed that the relative root growth of *fad*6 mutant plants was less than wild type at all concentrations of NaCl or KCl tested, indicating mutant seedlings are more sensitive to salt. Furthermore, the survival rate of seedlings harboring the *fad6-1* mutation was lower than wild type (~55% survival versus 70%, respectively)[56]. The Na^+ and K^+ contents of the seedlings were examined under normal and salt stress conditions and, although there was no difference in ion content in plants grown under normal conditions, upon treatment with 75 mM NaCl mutant plants accumulated significantly more Na^+ and less K^+ than wild type plants leading to an increased Na^+/K^+ ratio[56]. Further analysis of this mutant indicated it has increased electrolyte leakage and accumulated more malondialdehyde (MDA), an indicator for changes in lipid hydroperoxide and oxidative damage, than wild type plants under salt stress. Overall, the results of the study indicated that the disruption of *fad6* function seen in the mutant reduced its tolerance to salt-stress and induced membrane hyperperoxidation[56].

There is substantial evidence the trienoic fatty acids decreased in *fad6* mutant plants, 18:3 and 16:3, are essential for plant adaptation to cold stress. The loss of the ability to desaturate these fatty acids in the chloroplast has been shown to affect recovery from photoinhibition and chloroplast membrane biogenesis in mutants of *Arabidopsis*. In 2002, Vijayan and Browse used noninvasive chlorophyll florescence techniques to monitor the potential quantum yield of PSII (F_v/F_m) as a measure of photoinhibition and found that *fad6* mutant plants had about 26% greater photoinhibition when compared to wild type plants grown at 17°C[49]. In another study, analysis

of *fad6* mutant plants grown at 5℃ showed newly developed leaves had a chlorotic phenotype, containing only about half the chlorophyll of leaves from wild type plants. The severity of chlorosis varied with growth temperature, with mutants almost indistinguishable from wild type under standard growth conditions[48]. The chlorotic effect was not seen in fully expanded leaves after being transferred to low temperature, suggesting the phenotype is related to chloroplast development as opposed to a reduction in membrane stability. Comparison of the fatty-acid profiles of mutant and wild type plants grown at low temperature indicated they did not differ significantly, with both showing an increase in 18:3 at low temperature. At both temperatures, the *fad6* mutant showed characteristic increases in 18:1 and 16:1 fatty-acids with corresponding decreases in 18:3 and 16:3[48]. To evaluate the effect of low temperature on chloroplast development and ultrastructure in mutant vs. wild type plants, thin sections of chloroplasts were prepared from leaves that had expanded during growth at 5℃ and these sections were analyzed using electron microscopy. Analysis of the electron micrographs revealed chloroplasts from *fad6* mutant plants grown at 5℃ contained 70% less thylakoid membrane than chloroplasts from wild type plants grown at the same temperature. Moreover, the average cross sectional area from wild type vs mutant chloroplasts was notably reduced denoting a net reduction in the size of chloroplasts in mutant plants grown in the cold[48].

Further support for the role of polyunsaturated membrane lipids in chloroplast biogenesis came from a study by Xu et al. in 2010. In this study, a new allelic mutant of FAD6 (*fad6-2*) was identified from a restorer screen conducted on an ethane methyl sulfonate (EMS)-mutagenized population of *tgd1-2 dgd1* double mutant plants[24]. The *tgd* mutants were originally isolated as suppressors of the stunted growth phenotype exhibited by the *dgd1* mutant due to DGD

deficiency. Mutations in genes encoding *tgd* proteins on the *dgd-1* background indirectly activate a processive galactosyltransferase which produces DGD and oligogalactolipids, suppressing the stunted growth phenotype[57]. The *fad6-2 tgd1-2 dgd1* triple mutant identified in the screen was pale green and showed a notable reduction in levels of DGDG and TGDG. Sequencing the FAD6 gene on the *fad6-2 tgd2-1 dgd1* triple mutant background revealed a single nucleotide polymorphism (C-to-T) resulting in the substitution of a conserved proline (Pro225) with a serine[24]. This result led researchers to recognize that mutations in desaturases in the plastid or ER could be used as tools to probe lipid trafficking phenomenon involving the ER and plastid. In 2011, Fan and colleagues conducted another study, with the goal of providing evidence for the role of TRIGALACTOSYLDIACYLGLYCEROL (TGD) proteins in lipid trafficking between the ER and chloroplast, the idea being that if lipid trafficking between these two organelles were impaired in the *fad6-1* background it would affect chloroplast membrane biogenesis in double mutant plants[57]. The results showed *fad6-1 tgd1-1* and *fad6-1 tgd4-3* double mutant plants were chlorotic and had a significantly decreased ratio of plastidic-to-extraplastidic membranes under standard growth conditions. Ultrastructural analysis revealed the thylakoid membranes of double mutants were severely underdeveloped with negligible grana stacking, and the number of chloroplasts per cell were also significantly decreased[57].

In addition to being associated with decreased tolerance to cold and salt stress, mutations in the *fad6* gene have been shown to suppress stress response phenotypes resulting from mutations in other enzymes including *FATTY ACID BIOSYNTHESIS 1(FAB1)* and *FATTY ACID BIOSYNTHESIS 2 (FAB2)*(Table 1.1). The *fab1* mutant contains a mutation in a locus encoding β-ketoacyl-[ACP]-synthase II (KASII) which catalyzes the elongation of 16:0-ACP to 18:0-

ACP[58]. As a result, *fab*1 mutant plants have increased levels of 16:0 in all membrane glycerolipids, and levels of high-melting point species of PG comparable to chilling-sensitive plants. Like chilling-sensitive plants, *fab1* mutant plants show a collapse of photosynthesis and subsequent death after prolonged exposure to low temperature[59,60]. In 2015, Gao and colleagues identified the *fad6-1* mutation as a suppressor of *the fatty-acid biosynthesis 1 (fab1)* low temperature phenotype. Analysis of fatty-acids of the *fad6-1 fab1* double mutant revealed the 16:0 levels of the double mutant were significantly lower than the *fab1* mutant but still higher than wild type plants, supporting the conclusion that increased levels of 16:0 are responsible for the *fab1* cold phenotype[61]. The *fab2* mutant (also known as *"ssi2"* mutant) contains a mutation in a gene encoding a stearoyl-acyl carrier protein desaturase (S-ACP-DES) which results in a 10-fold increase in the steric acid (18:0) content of mutant plants. The recessive mutation results in constitutive expression of genes encoding pathogen-resistance related (PR) proteins, spontaneous lesions, and increased resistance to bacterial and oomycete pathogens. On the other hand, some defense responses regulated by the JA signaling pathway are impaired including expression of *PDF1.2* (a defensin gene) and resistance to *Botrytis cinerea*[20]. In 2003, Nandi et al. and Kachroo and colleagues found that mutations in the chloroplast localized enzymes FAD6 and glycerol-3-phosphate acyltransferase (ACT1) could suppress or partially suppress various *fab2* triggered phenotypes[,62,108]. Unlike *fab2*, double-mutant plants with the *act1* mutation (*act1/fab2*) did not show constitutive expression of PR proteins or spontaneous cell death, and they did not show induction of PDF1.2 indicating the mutation is sufficient to revert *fab2* plants to wild-type-like plants. The *fad6* mutation, on the other hand, resulted in only partial reversion of *fab2* defense signaling phenotypes[62]. Double mutants of *fad6-1 fab2* were much larger than *fab2* plants but smaller than wild-type. They showed no visible lesions on their leaves but did show microscopic

cell death. Double mutant plants expressed high levels of PR genes, like those found in *fab2* mutant plants, indicating the *fad6* mutation is not sufficient to revert cell death or PR gene expression phenotypes of *fab2* plants[62]. The *fad6-1 fab2* leaves that showed reduced numbers of dead cells showed slightly higher expression of *PDF1.2* which was still significantly lower than wild-type, *fad6,* or *act1 fab2* suggesting the partial rescue of the phenotype by the *fad6-1* mutation. The levels of 18:1 in *fad6-1 fab2* mutant plants were ~25-fold greater than in *fab2* mutant plants and ~10-fold greater than in *act1 fab2,* suggesting increases in the 18:1 content of chloroplast membranes is not sufficient to completely revert defense signaling phenotypes seen in the *fab2* mutant[62].

In this study, we have identified a new allelic mutant of FAD6 (*fad6-3*) on the background of *Arabidopsis* T-DNA insertion line SALK_109175C, which has a known insertion in the gene *At5g64790*. Lipid analysis of leaves from this insertion line revealed a decreased ratio between two monogalactocyldiacylglycerol molecular species, MGDG(18:3/16:3) and MGDG(18:3/18:3), as well as other alterations in chloroplast-assembled lipid species. This lipid phenotype did not co-segregate with the known insertional mutation, and genetically mapped to a region containing the *At4g30950* locus which encodes the plastid localized ω6 fatty acid desaturase FAD6. Sequencing of *fad6-3* genomic DNA revealed a splice site mutation between exons 9 and 10 and sequencing of cDNA revealed an in-frame deletion of 13 amino acids on the C-terminal end of the protein. Comparison of the deleted sequence across species revealed multiple amino acids that are conserved among species of plants and even cyanobacteria. In this study, we cloned and heterologously co-expressed wild type *AtFAD6* with several constructs of a photosynthetic ferredoxin from *Arabidopsis* (*AtFD2*) in yeast under the control of a constitutive

promoter (CDC11) or an induced promoter (Gal1/10) with the goal of determining which combination of gene and promoter results in the highest activity. The future of this project involves cloning and expressing *fad6-1, fad6-2, and fad6-3* sequences in addition to *FAD6* C-terminal truncations and other constructs in yeast to evaluate the impact of conserved residues on enzyme function. In conducting this study, we hope to elucidate the function of the conserved residues, and expand knowledge about the molecular mechanisms and substrate specificity of integral membrane desaturases, including FAD6.

Gene	Name(s)	Position	Substrate(s)	Location	Integral membrane?	Annotation Score	References
AT2G43710	*Fatty-acid biosynthesis 2 (FAB2, SSI2)*	Δ9	Stearoyl-ACP	Chloroplast	N	5	3-8
AT3G12120	*Fatty acid desaturase 2 (FAD2)*	Δ12	18:1 on PC	ER	Y	5	64-71
AT2G29980	*Fatty acid desaturase 3 (FAD3)*	Δ15	18:2 on PC	ER	Y	4	72,73
AT4G27430	*Fatty acid desaturase 4 (FAD4, FADA)*	Δ3 *trans*	16:0 on PG	Chloroplast	Y	5	74,75
AT3G15850	*Fatty acid desaturase 5 (FAD5, FADB)*	Δ7	16:0 on MGDG	Chloroplast	Y	5	76
AT4G30950	*Fatty acid desaturase 6 (FAD6, FADC)*	Δ12 Δ10	18:1 on PG, MGDG, DGDG, or SQDG; 16:1 on MGDG	Chloroplast	Y	5	55
AT3G11170	*Fatty acid desaturase 7 (FAD7, FADD)*	Δ15 Δ13	18:2 on PG, MGDG, DGDG, or SQDG 16:2 on MGDG	Chloroplast	Y	5	77
AT5G05580	*Fatty acid desaturase 8 (FAD8)*	Δ15 Δ13	18:2 on PG, MGDG, DGDG, or SQDG 16:2 on MGDG	Chloroplast	Y	4	78
AT1G06090	*Delta-9 desaturase-like 1 protein*	Δ9	N/A	ER	Y	2	N/A
AT1G06100	*Delta-9 desaturase-like 2 protein*	Δ9	N/A	ER	Y	2	N/A
AT1G06120	*Delta-9 desaturase-like 3 protein*	Δ9	N/A	ER	Y	2	N/A
AT1G06350	*Delta-9 desaturase-like 4 protein (ADS4)*	Δ9	N/A	ER	Y	2	N/A
AT1G06360	*Delta-9 desaturase-like 5 protein*	Δ9	N/A	ER	Y	2	N/A
AT3G15870	*Probable lipid desaturase (ADS3.2)*	N/A	N/A	Chloroplast	Y	3	79

Table 1.1 Fatty acid desaturase encoding genes in the model plant *Arabidopsis thaliana* according to The Arabidopsis Information Resource (www.arabidopsis.org). Note the addition of 16-carbon substrates for FAD6, FAD7, and FAD8. The annotation score is a heuristic measure of the annotation content of a UniProtKB entry or proteome. Scores range from 1 to 5, with 5 indicating the best annotation (www.uniprot.org/help/annotation_score).

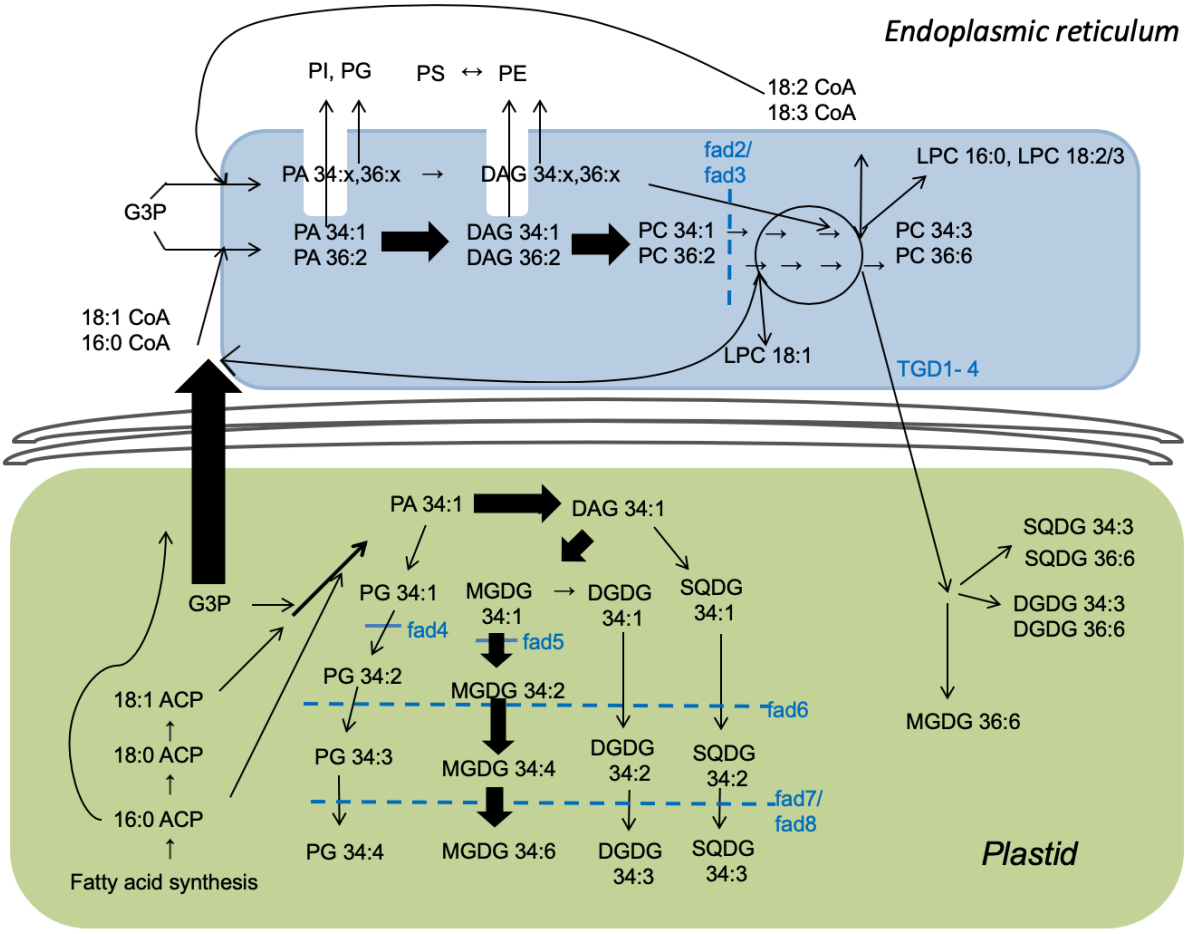

Figure 1.1 An abbreviated diagram of the two-pathway scheme for glycerolipid synthesis in 16:3 plants. The width of the lines represent relative fluxes. Image adapted from Maatta et al. 2012[63].

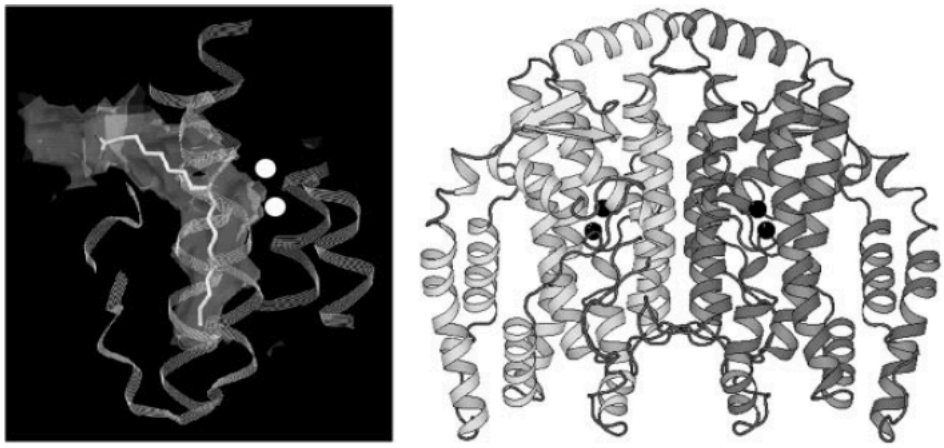

Figure 1.2 Structural representation of the castor Δ9-18:0-ACP desaturase. Desaturase dimer (right); two subunits are represented by light or dark shading, the black spheres represent iron ions. Expanded view shows the relationship of helices to the substrate-binding pocket (left); stearic acid is modeled into the pocket and iron ions are represented by white sphere[35].

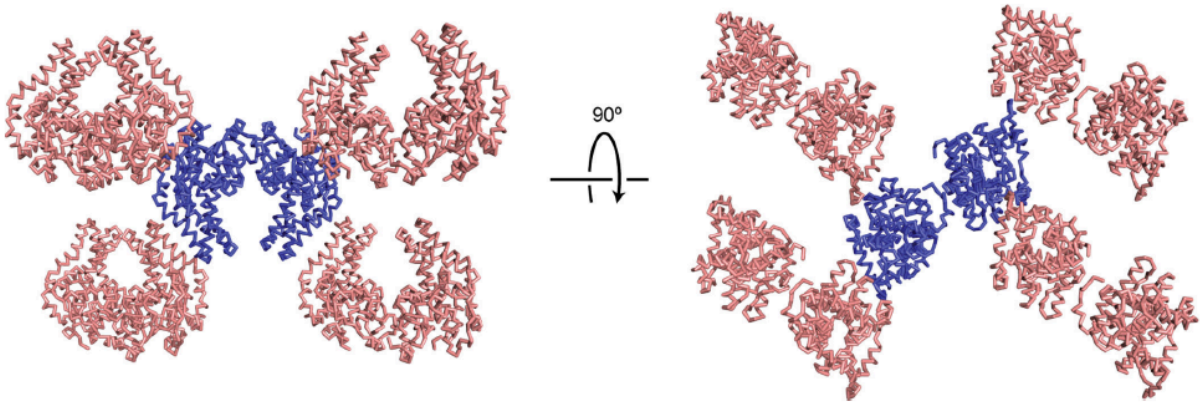

Figure 1.3 Cross-sections of the crystal lattice for mouse SCD1 lipidic cubic phase crystals, viewed from two perpendicular directions. One asymmetric unit is colored blue[42].

Chapter 2 - Identification and characterization of C-terminal alterations in *Arabidopsis thaliana* FATTY ACID DESATURASE 6 (FAD6)

Introduction

FATTY ACID DESATURASE 6, or FAD6, is an ω6-fatty acid desaturase which catalyzes the introduction of a double bond in the biosynthesis of 16:3 and 18:3 fatty acids in the chloroplast (Figure 1.1 and Table 1.1). It is an integral-membrane protein of 418 residues and ~48,000D, residing in the chloroplast inner membrane and using soluble ferredoxin as an electron donor. FAD6 has been shown to be involved in chloroplast membrane biogenesis[48,80] and plant adaptation to stresses including cold stress[48] and salt stress [56]. It has also been shown to suppress and rescue phenotypes of other *Arabidopsis* mutants, *fatty acid biosynthesis1 (fab1)* in the cold[61] and *fatty acid biosynthesis2* (*fab2*, and also known as *ssi2*) in growth and with defense ramifications[6], although the underlying mechanism remains unclear. FAD6 is involved in the biosynthesis of highly unsaturated trienoic fatty acids attached to PG, SQDG, and galactoglycerolipids MGDG and DGDG characteristic of the thylakoid membrane, an organelle in the chloroplast where the light-based reactions of photosynthesis occur. *FAD6* mutants have a chlorotic phenotype during cold stress, with alterations in chloroplast organization and ultrastructure in newly developed leaves[48]. Despite the abundance of sequence information, structural data and functional analysis on this desaturase are lacking and are needed to fully understand its molecular function. Our understanding of membrane-bound desaturases, in general, has lagged behind that of soluble desaturases largely due to technical challenges with structural analysis and direct functional investigation.

The characterization of plant microsomal fatty acid desaturases (FADs) is typically achieved through cloning and heterologous expression, although optimal conditions for expression are still be delineated. Yeast (*Saccharomyces cerevisiae)* is often employed because it uses cytochrome b_5 and cytochrome b_5 reductase as electron donors[81,82]. However, for plastidial FADs, cyanobacteria are generally regarded as a more suitable system because they contain the required ferredoxin and ferredoxin reductase[83,84]. Unfortunately, cyanobacteria may not provide optimal conditions for all plastidial FADs due to limitations, including availability of substrate *in planta*[85-87]. A study by Domergue and colleagues in 2003 demonstrated that yeast cells supplied with linoleic acid (18:2) rapidly incorporated the fatty acid at both the sn-1 and sn-2 position of neutral and polar lipids, in contrast to cyanobacteria[88], making them more suitable for the expression of some plastidial FADs. The same lab reported low activity for a plastidial ω6-desaturase, similar to *Arabidopsis* FAD6, heterologously expressed in yeast[89]. In 2009, Venegas-Calerón et al. reported that co-expressing a plastidial ω3-desaturase from sunflower (HaFAD7) in yeast with photosynthetic ferredoxin from the same species (Hafd1) resulted in a 10-fold increase in activity compared to the desaturase alone, although the observed activity was still very low[87]. In another study, the same lab co-expressed several different constructs of HaFAD7 with Hafd1 in yeast to determine whether the low activity resulted from suboptimal interactions with co-factors or mistargeting and degradation of the enzyme in the absence of chloroplast membranes. They generated several different constructs in which the first 51 amino acids (representing the transit peptide) were deleted and replaced with domains known to target proteins to the ER membrane in yeast. In some constructs, a KKNL-stop motif was also introduced at the C-terminus to ensure ER-retention of mutant proteins. The analysis revealed

that removal of the chloroplast targeting sequence and addition of the ER-retention signal resulted in a 10-fold increase in activity for FAD7-KKNL compared to WT-FAD7 with the native transit sequence, supporting the conclusion that low activity was due to mistargeting and degradation of the protein [86].

In this study, we identified a new allelic mutant of *FAD6* (*fad6-3*) in the background of *Arabidopsis* T-DNA insertion line SALK_109175C using map-based (positional) cloning. Sequencing of *fad6-3* genomic DNA revealed a splice site mutation between exons 9 and 10 and sequencing of the corresponding cDNA showed an in-frame deletion of 13 amino acids. Comparison of the deleted sequence across species revealed that multiple amino acids in this region are conserved across plants and even in cyanobacteria. In this study, we generated constructs of wild type *AtFAD6* lacking the signal peptide with the added di-lysine motif KEK (endogenous to HaFAD7) and ER retention signal KKNL, and co-expressed them in yeast with several constructs of a photosynthetic ferredoxin from *Arabidopsis* (*AtFD2*) with and without the chloroplast transit peptide. *AtFAD6* and *AtFD2* constructs were alternately co-expressed under the control of a constitutive promoter (CDC11) or an induced promoter (Gal1/10). The goal was to determine which combination of construct and promoter results in the highest activity. Future experiments will use the yeast system to test the function of *fad6-1, fad6-2, and fad6-3* sequences in addition to *fad6* C-terminal truncations and other constructs to evaluate the impact of mutating conserved residues on enzyme function. In conducting this study, we hope to elucidate the function of the conserved residues, and expand our understanding of the molecular mechanisms and substrate specificity of integral membrane desaturases.

Materials and Methods

Plant materials and growth conditions

Arabidopsis thaliana accession Columbia-0 (Col-0) and Salk_109175C seeds obtained from The Arabidopsis Biological Resource Center (ABRC, Ohio State University, Columbus, Ohio). were sown at 3 seeds per well in 72-well plug trays (Hummert International, Earth City, MO, USA) filled with loosely packed, autoclaved and cooled Pro-Mix "PGX" soil (Hummert International, Earth City, MO, USA) saturated with 0.01% Jacks All Purpose 20-20-20 fertilizer (J.R. Peters Inc., Allentown, PA, USA). After trays were sown they were covered with propagation dome lids and incubated at 4 ℃ for 2 days before transfer to a growth chamber under a 14/10h light/dark cycle at 21℃ with 60% humidity. Light intensity was maintained at 5500-6500 lux. Propagation dome lids covered the plants for the first 9 days to maintain high humidity. Trays were watered on days 11, 16, 24 and 28. On day 13 after sowing, plants were thinned to one plant per well. On day 20, trays were fertilized again with 0.01% Jacks All Purpose 20-20-20 fertilizer (J.R. Peters Inc., Allentown, PA, USA). Leaves for lipid analysis were harvested on day 30.

Lipid extraction and instrument parameters for analyses

Lipids were extracted from leaf 4 of 30 day old plants and analyzed using the method described in Welti et al. (2002)[15]. The lipid analytical procedure for broad-based lipid analysis used multiple reaction monitoring as described by Vu et al[109]. The global settings for those analyses on the Xevo TQ-S mass spectrometer were: capillary voltage, ±2.8 kV; source offset voltage, ±30.0 V; cone voltage, ±40.0 V; source temperature, 150°C; desolvation temperature, 250°C; cone gas flow, 150 L h-1; desolvation gas flow, 650 L h-1; collision gas flow, 0.1 ml min^{-1};

nebulizer gas pressure, 7 bar; low mass 1 and 2 resolution, 2.5; and high mass 1 and 2 resolution, 14.5; ion energy 1 and 2, 1.0. Interchannel delay (ICD) was 0.006-0.012 s in positive mode and 0.100 s in negative mode. Interscan delay (ISD) was 0.020 s in positive mode and 0.100 s in negative mode. When only MGDG molecular species analyses were analyzed, such as in screening F2 plants in the cross of Col-0 X Salk_109175C, a neutral loss of 179 scan was used, as described by Xiao et al., 2010[110].

Genetic Analysis of Col-0 X Salk_109175C F2

DNA was extracted from leaf 5 of 30-day old wild type (Col-0) *Arabidopsis* and Salk_109175C plants using the protocol described in Edwards et al.[90] . Plants were genotyped as wild type, heterozygous, or homozygous for the known T-DNA insertional mutation using Salk_109175C-F (5'-AGATTTCACCGGACAAGGAC-3'), Salk_109175C-R (5'-TCTTCCGAACACAAAGTTGATCC-3') and LBb1.3 (5'-GGACCGCTTGCTGCAACT-3'). Individual PCR reactions contained 7.5 μl of 2x Econotaq PCR master mix (Lucigen, Middleton, WI), 1 µl DNA, 1.2 µl forward and reverse primers and 4.1 µl distilled water and were amplified on a Bio-Rad T100 thermal cycler (Bio-Rad Laboratories, Inc. Hercules, CA) using the following amplification protocol: 2-min polymerase activation and denaturation at 94℃, and 35 cycles of 94℃ for 30 s, 55℃ for 30 s, and 72℃ for 2 min and 30 s, followed by a final extension at 72℃ for 5 min.

Map-based Cloning

Map-based (or positional) cloning was achieved by crossing the mutant, on a Columbia (Col-0) background, to Landsberg *erecta* (Ler-0), creating an F2 mapping population, and following the

mapping procedure outlined by Lukowitz et al. [91]. Sequences for flanking PCR markers were obtained from the Arabidopsis Mapping Platform (http://amp.genomics.org.cn/)[92]. The sequences of the markers used in this study are listed in **Table S.1**.

Amplification and sequencing of *FAD6* genomic DNA

Full length genomic *FAD6* was amplified using DNA extracted from wild type (Col-0) and *fad6-3* leaves using the primers FAD6 5'UTR-F (5'-GCTGAAGAAGGTGAAGAGGTGAG-3') and FAD6 3' UTR-R (5'-GTGTTAGAGAAGCTCATCGCTTGG-3'). Individual PCR reactions contained 10 μl 5x Phusion HF buffer (Thermo Fisher Scientific, Waltham, MA), 10 mM dNTPs (New England Biolabs, Ipswich, MA), 2.5 μl forward and reverse primers, and 0.5 μl Phusion HF enzyme (Thermo Fisher Scientific, Waltham, MA). The Col-0 reaction contained 3 μl template DNA and 30.5 μl water whereas the *fad6-3* reaction contained 1 μl template DNA and 32.5 μl distilled water. Samples were amplified on a Bio-Rad T100 thermal cycler (Bio-Rad Laboratories, Inc. Hercules, CA) using the following amplification protocol: 30 s polymerase activation and denaturation at 98℃, and 35 cycles of 98℃ for 10 s, 59℃ for 30 s, and 72℃ for 2 min and 30 s, followed by a final extension at 72℃ for 10 min. After amplification PCR products were run on a 1% agarose gel + 3 μl ethidium bromide at 120 volts for 60 min. Bands were cut from the agarose gel and DNA fragments amplified by PCR were extracted and purified using QIAquick gel extraction kit (Qiagen, Hilden, Germany). After amplification and purification, samples were sent to Genewiz (Genewiz, Plainfield, NJ) for Sanger sequencing using sequencing primers FAD6seq1(5'-CGGATTGCAATAATGAATGC-3'), FAD6seq2(5'-CGGCTTCACAGCATATATACACC-3'), FAD6seq3(5'-GGTAAGCTCTCCTCCACTG-3'),

FAD6seq4(5'-GGTGGCCACTGATCGTATAC-3'), and FAD6seq5(5'-GGCTACATGGAACTGGCG-3').

Plant growth conditions for RNA extraction

To grow plants for RNA extraction, *Arabidopsis* seeds were sterilized by chlorine gas treatment and sown onto 0.8% agar (plant tissue culture grade) containing 1X Murashige and Skoog medium 60, 1% sucrose, and 0.5% MES buffer at pH 5.8. Seeds were transferred to 21°C and grown under continuous light for 12 days, at which time they were transferred to 72-well plug trays (Hummert International, Earth City, MO, USA) filled with loosely packed, autoclaved and cooled Pro-Mix "PGX" soil (Hummert International, Earth City, MO, USA) saturated with 0.01% Jacks All Purpose 20-20-20 fertilizer (J.R. Peters Inc., Allentown, PA, USA) and grown for another 18 days. Plants were watered on days 16, 24, 28, and fertilized on day 20. Leaf tissue samples for RNA extraction were taken on day 30.

RNA extraction and cDNA synthesis

Tissue samples were taken from leaf 5 of 30-day-old wild-type (Col-0) and *fad6-3* plants. Tissue samples were frozen in liquid nitrogen and stored at -80°C prior to RNA extraction with the RNeasy Plant Mini Kit and on-column RNase-Free DNase Set (Qiagen, Hilden, Germany). RNA was quantified by measuring absorbance at 260 nm. Total RNA (0.5 μg) was used as a template for cDNA synthesis. The first-strand cDNA synthesis was performed with Oligo (dT) primer using GoScript Reverse Transcriptase (Promega, Madison, WI).

Amplification and sequencing of *FAD6* cDNA

FAD6 cDNA was amplified using the primers FAD6 5'UTR-F (5'-GCTGAAGAAGGTGAAGAGGTGAG-3') and FAD6 3' UTR-R (5'-GTGTTAGAGAAGCTCATCGCTTGG-3'). Individual PCR reactions contained 10 μl 5x Phusion HF buffer (Thermo Fisher Scientific, Waltham, MA), 10 mM dNTPs (New England Biolabs, Ipswich, MA), 2.5 μl forward and reverse primers, 1 μl template cDNA, 32.5 μL distilled water, and 0.5 μl Phusion HF enzyme (Thermo Fisher Scientific, Waltham, MA). Samples were amplified on a Bio-Rad T100 thermal cycler (Bio-Rad Laboratories, Inc. Hercules, CA), using the following amplification protocol: 30 s polymerase activation and denaturation at 98℃, and 35 cycles of 98℃ for 10 s, 59℃ for 30 s, and 72℃ for 2 min and 30 s, followed by a final extension at 72℃ for 10 min. After amplification PCR products were run on a 1% agarose gel + 3 μl ethidium bromide at 120 volts for 60 min. Bands were excised from the agarose gel and DNA fragments amplified by PCR were extracted and purified using a QIAquick gel extraction kit (Qiagen, Hilden, Germany). After amplification and purification samples were sent to Genewiz (Genewiz, Plainfield, NJ) for Sanger sequencing, using primers FAD6seq4(5'-GGTGGCCACTGATCGTATAC-3'), and FAD6seq5(5'-GGCTACATGGAACTGGCG-3').

Quantification of gene expression by quantitative Real-Time PCR (qRT-PCR)

Real-time PCR was performed using iTaq SYBR Green Supermix with the CFX96 Touch Real-Time PCR Detection System (Bio-Rad, Hercules, CA). Each reaction contained 10 µl of SYBR Green Supermix, 1 µl of forward and reverse 10 mM gene-specific primers, and 5 µl of cDNA (diluted 5-fold) in 20 µl. Standard curves were generated from 10-fold dilutions of amplicons for each primer pair. *ACT7* served as the reference gene. The qPCRFAD6-F (5'-

GGACAGGAACTGCAATTACCGG-3'), and qPCRFAD6-R (5'-GAGTACCCACAATGTCTTCCACC-3'), ACT7-F (5'-TCGCACATGTACTCGTTTCGCTTTC-3')[93] and ACT7-R (5'-TCGAGAAGCAGCGAGAGAGAAAGATAGA-3')[93] gene-specific primers were used for PCR amplification of *FAD6* and *ACT7,* respectively.

Sequence alignments and structural modeling

Alignment of amino acid sequences for ω6-desaturase proteins was done using Clustal X v.2.0[94] with the default setting. Protein structural modeling was done using I-TASSER (Iterative Threading ASSEmbly Refinement)[95-97].

Arabidopsis *FAD6* and *FD2* plasmid construction

Standard molecular biology techniques were used for strain and plasmid construction[98] .
The *atFAD6* protein sequence lacking the chloroplast transit peptide with added residues KEK-KKNL (for ER localization) + N-terminal HA tag and the *atFD2* protein sequence + C-terminal HA tag were codon optimized for expression in *S. cerevisiae* and synthesized by GenScript (GenScript, Piscataway, NJ). Plasmids used in this study can be found in Table S4. For plasmid construction, plasmids pRS316[99] and pRS315[99] were digested with SpeI-HF (New England Biolabs, Ipswich, MA) and Not1-HF (New England Biolabs, Ipswich, MA), respectively. The general strategy for strain construction was first to use *in vivo* ligation and homologous recombination [100-103] to generate a plasmid containing the gene of interest (or an epitope- protein-tagged derivative) under the control of a promoter and terminator of choice (Gal1/10 or CDC11), and harboring a juxtaposed MX-based drug cassette[104]. Primer sequences used to amplify

fragments for *in vivo* ligation are listed in Table S3 and a visual representation of each plasmid assembly can be found in Figures S5 and S6. Plasmids used in this study are listed in Table S4.

Culture conditions

Yeast strains were grown at 30℃ in rich medium (YPD), or synthetic medium (SD) supplemented with the appropriate amino acids and/or other nutrients and glucose/dextrose (2%) as the carbon source. Where indicated, filtration-sterilized (not autoclaved) galactose (2%) was the carbon source.

Functional expression in yeast

The generated plasmids were transformed into the *S. cerevisiae* strain INVSc1 (Invitrogen, Carlsbad, CA) using the lithium acetate method[105]. Transgenic yeast cells were grown at 30℃ synthetic media ($SD^{-Ura-Leu}$) supplemented with the appropriate amino acids and expression of the transgenes was induced by the addition of galactose to 2% (w/v).

Yeast lipid extraction and analysis

Cells were lysed by vortexing for 5 min with ~500 µl 45 mm diameter Zirconia/silica beads (BioSpec Products, Inc., Bartlesville, OK). Lipids were extracted by adding one part chloroform and 2 parts methanol to 0.8 parts lysed yeast cells in aqueous solution. Samples were vortexed and centrifuged for 5 min. The lower layer was removed and saved. This process was repeated twice and the combined lower layers were used for making fatty acid methyl esters (FAMEs). Total fatty acids extracted from yeast cultures were analyzed by gas chromatography (GC) of

methyl ester derivatives[106] . Fatty acids were identified by comparison with the retention times of fatty acid methyl ester (FAME) standards (Sigma) and by GC–mass spectrometry (MS)[107].

GC-flame ionization detector (GC-FID) method

FAME analysis was performed on an Agilent 6890N GC coupled to a FID (flame ionization detector). The GC was fitted with a DB-23 capillary column (column length - 60 m, internal diameter - 250 µm, film thickness - 0.25 µm). Helium was used as the carrier gas at a flow rate of 1.5 ml/min. The back inlet was operating at a pressure of 36.01 psi and 250°C temperature. An Agilent 7683 autosampler was used to inject 3 µL of the sample in the splitless mode. The GC oven temperature ramp was operated as follows: initial temperature of 150 °C, held for 1 min, increased at 25 °C/min to 175 °C, then increase at 4°C/min to 230°C and held 8 min. Total run time was 23.75 min. The FID detector was operated at 260 °C. The hydrogen flow to the detector was 30 ml/min and air flow was 400 ml/min. The sampling rate of the FID was 20 Hz.

GC-MS method

GC-MS was performed on an Agilent 6890N GC coupled to an Agilent 5975N quadrupole mass selective detector. The GC was fitted with a VF-5MS capillary column (inert 5% phenylmethyl column, length: 30 mm, internal diameter: 250 µm, film thickness: 0.25 µm) with a 10 m EZ guard column. Helium was used as the carrier gas at a column flow rate of 1 ml/min. The front inlet was operated at 250°C. The Agilent 7683 autosampler was used to inject 1 µL of the sample in the splitless mode. The GC oven temperature program was: initial temperature of 150 °C, held for 1 min, and increased at 5°C/min to 300°C. The total run time was 31 min. The mass spectrometer was operated in the electron impact mode at 70 eV ionization energy. The MS

quad temperature was 150°C, and the MS source temperature was 230°C. The data acquisition was in scan mode. The scanned mass range was 50 to 650. The data were processed with Agilent Chemstation software.

Results and Discussion

Salk_109175C has low levels of chloroplast assembled membrane glycerolipids.

Lipid analysis of the T-DNA insertion line SALK_109175C, which has a confirmed mutation in *At5g64790*, a poorly characterized gene annotated as an O-glycosyl hydrolase, revealed significant changes in several monogalactocyldiacylglycerol (MGDG) species as well as other alterations, indicating altered chloroplast glycerolipid composition. Among the changes in SALK_109175C, compared to wild-type plants, were significant decreases in chloroplast assembled MGDG(18:3/16:3) (MGDG(34:6)) with corresponding increases in MGDG(18:3/18:3) (MGDG(36:6)) (Figure 2.1). There were also changes observed in other species of MGDG including MGDG(34:5), MGDG (34:4), MGDG(34:3), MGDG(35:3), and MGDG (36:4) (Figure 2.1). Other classes altered in mutant plants include DGDG (Fig. S1), SQDG (Fig. S2), and PG (Fig. S3). As in MGDG, DGDG's ratio of 34:6 to 36:6 species was lower in leaves of Salk_109175C than in leaves of wild type plants. SQDG(34:3) levels were also decreased in the mutant (Figure S3). Marked increases in PG(34:2) were observed with corresponding decreases in PG(34:4) (Figure S3). Taken together, the data indicate decreases in the levels of several chloroplast assembled glycerolipid species. The lipid changes observed in this mutant did not have a clear connection to glycosyl hydrolase activity. They do, however, resemble lipid changes previously described in mutants of plastid-localized acyl-transferases and

desaturases. Moreover, *At5g64790* is expressed primarily in pollen, whereas the lipid changes are observed in the leaves.

The mutant lipid phenotype does not co-segregate with the *At5g64790* T-DNA insertional mutation.

Salk_109175C has a confirmed mutation at the *At5g64790* locus, a gene which is mostly expressed in pollen. However, the lipid phenotype was observed in leaves. To determine whether the phenotype was due to the known insertional mutation, the homozygous Salk line was crossed with wild type (Col-0), and an F2 generation was obtained. The phenotypes of F2 plants were compared to their respective genotypes to determine if the phenotype co-segregated with the known T-DNA insertion mutation. The analysis indicated that the phenotype of low MGDG(34:6)/ MGDG(36:6) was found in plants wild type, heterozygous, and homozygous for the Salk_109175C *mutation* at the *At5g64790* locus (Figure 2.1). This finding indicated the low MGDG(34:6)/ MGDG(36:6) phenotype is not related to the known insertion mutation in Salk_109175C. Additionally, the heterozygous F1 progeny of a cross between the wild type and mutant line had an intermediate lipid phenotype, indicating the wild type allele is semi-dominant.

The mutation mapped to the *At4g30950* locus which encodes the plastid-localized *ω*6 desaturase FAD6.

Map-based (or positional) cloning was used to map the gene associated with the observed lipid compositional changes. An F2 plant with the low MGDG(18:3/16:3) lipid phenotype, but without the known T-DNA insertional mutation, was crossed to accession Landsberg *erecta* (Ler-0) Arabidopsis and F1 plants were allowed to self-pollinate to obtain an F2 generation. An

F2 mapping population was generated by identifying F2 plants with the low MGDG(18:3/16:3) lipid phenotype and extracting DNA for use in mapping. To find the locus associated with the lipid phenotype, we identified the F2 mutant plants with the low MGDG(18:3/16:3) lipid phenotype by mass spectral analysis, and searched among these plants for the chromosomal location that consistently was Col-0 (since the mutation causing the phenotype came from Col-0). Markers used for mapping the mutation were obtained from the Arabidopsis Mapping Platform (http://amp.genomics.org.cn/)[92]. The sequences of the markers used are listed in Table S.1. The mutation associated with the lipid compositional phenotype mapped to a 2.1 mB area on chromosome 4 that included the *At4g30950* locus which encodes the plastid-localized ω6 fatty acid desaturase FAD6. Sequencing the full-length *FAD6* gene showed a single nucleotide polymorphism (SNP) at the acceptor splice site between exons 9 and 10. cDNA sequencing revealed that the G to A transition at bp1,075 of *FAD6* genomic DNA, termed *fad6-3*, resulted in the in-frame deletion of the first 13 amino acids of exon 10 near the C-terminus of the protein (Figure 2.2). This deletion is downstream of the three histidine boxes and four transmembrane domains in a region that has not been functionally characterized (Figure 2.2). However, the lipid phenotype of *fad6-3* is consistent with known *FAD6* loss-of-function mutations *fad6-1* and *fad6-2* [54,24] (Table 2.1), suggesting it is also a loss-of-function mutation (Figure S4).

Multiple residues within the deletion are conserved among plants.

To determine if the amino acid sequence in this region is conserved in other plastidal ω-6 desaturases, we compared the Arabidopsis FAD6 amino acid sequence with similar sequences from other plants revealed multiple amino acids in the deleted sequence are conserved in FAD6 desaturases between Arabidopsis and rice. Four amino acids in Arabidopsis FAD6 (Tyr405,

Trp413, Leu415, and Lys417) are conserved in the aligned ω6-desaturases from rice (*Oryza sativa*), and cyanobacteria (*Synechocystis). Arabidopsis* ER-localized ω6-desaturase FAD2 (Figure 2.2), which is 24% identical and 49% similar to Arabidopsis FAD6[55] shares only Tyr at a position corresponding with Tyr405 with FAD6 and the aligned rice and cyanobacterial sequences.

Expression of *FAD6* mRNA is not affected in *fad6-3* mutants.

Real-time PCR data suggest there is no significant difference in *FAD6* expression at the transcriptional level in the leaves of *fad6-3* mutants when compared to wild type (Figure 2.3). This result is consistent with the previously described *FAD6* mutant *fad6-1*[55], perhaps suggesting no regulatory mechanism exists to increase transcriptional expression of the *FAD6* gene in response to decreased polyunsaturation in thylakoid membrane lipids.

Expression of *FAD6* led to the production of 18:2 in *Saccharomyces cerevisiae*

The design of *AtFAD6* constructs used in this study were based on a publication by Venegas-Calerón et al.[86] in which the activity of a plastidial integral membrane fatty acid desaturase from sunflower (HaFAD7) expressed in yeast was increased over 10-fold by deleting the chloroplast signal peptide and incorporating an ER retention signal KKNL. For *AtFAD6* constructs, a di-lysine (KEK) motif, endogenous to the C-terminus of *HaFAD*7 but not *AtFAD6*, was added along with the ER retention signal (KKNL) (Figure 2.4) to promote stable accumulation of the protein to the ER in yeast[86]. Venegas-Calerón and colleagues also showed N-terminally tagged *HaFAD7* had higher activity than the C-terminally tagged protein, suggesting the C-terminal tag interfered with activity[86]. Since the integral-membrane proteins (FAD7 and FAD6) are

structurally similar, HA epitope-tagged *AtFAD6* was constructed with the tag incorporated on the N-terminus (Figure 2.4). Previous studies have demonstrated plant plastidial FADs require co-expressed ferredoxin for activity[87], but none have examined the effect of the ferredoxin chloroplast transit signal on localization and activity. To this end, *AtFD2* constructs were designed with and without the transit signal to evaluate its impact on activity. The epitope tagged versions of *AtFD2* had the tag incorporated on the C-terminus (Figure 2.4). To determine which combination of *AtFAD6* and *AtFD2* constructs co-expressed in yeast yielded the highest enzymatic activity, each of the constructs marked with an asterisk in Figure 2.4 was co-expressed under the control of the galactose induced Gal1/10 promoter (vector pRS316) or the constitutive CDC11 promoter (vector pRS316). Plasmids (listed in Table S.4) were transformed into yeast (strains listed in Table S.5) and expression was induced by the addition of galactose.

In *Arabidopsis,* the native substrates for *AtFAD6* are 18:1 or 16:1 at the sn-1 or sn-2 positions of glycerolipids, phospholipids, and sulfolipids in the chloroplast. The plastidial desaturase *AtFAD6* does not appear to be specific to the lipid head group, chain length, or chain position, but does require a previously existing double bond at Δ9 in 18:1 or Δ7 in 16:1 for catalysis. The 16:1 FAs endogenous to wild type yeast have a double bond at Δ9, rather than Δ7, so the enzyme was expected to act only on 18:1 in yeast. Wild type yeast does not make linoleic acid (Δ9,Δ12-18:2), the product of FAD6 desaturation. Fatty-acid methyl esters (FAMEs) from transgenic yeast were screened for 18:2 production to evaluate enzymatic activity. GC-FID analysis of FAME's from transgenic yeast revealed heterologous co-expression of *AtFAD6* and *AtFD2* led to the production of linoleic acid in each of the strains tested. As expected, no linoleic acid was detected in wild type yeast (INVSc1) (Figure 2.4). Moreover, the highest level of 18:2

production was seen in the yeast strain with *AtFAD6* under the control of the galactose induced promoter (GAL1/10) and *AtFD2* under the control of the constitutive promoter (CDC11) (Figure 2.4). The chloroplast signal peptide on *AtFD2* did not appear to have a notable impact on activity (Figure 2.4). Since activity was observed in all transgenic yeast strains tested, the epitope-tagged constructs were not used because 18:2 production was observed, indicating the heterologously expressed desaturases are localized to the ER.

Conclusion

In this study, we identified a new allelic mutant of *Arabidopsis FATTY ACID DESATURASE 6 (FAD6),* termed *fad6-3*, on the genetic background of T-DNA insertion line Salk_109175C obtained from the Arabidopsis Resource Center (ABRC) using map-based (or positional cloning). We sequenced and identified the mutation as a G to A transition at bp1,075 of *FAD6* genomic DNA, which results in the in-frame deletion of the first 13 amino acids of exon 10 near the C-terminus of the protein. Interestingly, this deletion is downstream of the main structural components of the desaturase in an area not known to be functionally relevant, but the lipid phenotype is consistent with previously described FAD6 loss-of-function mutations**,** suggesting is also loss-of-function. Comparing the deleted sequence with those from FAD6 homologs revealed multiple amino acids in the region are conserved in FAD6 desaturases in plants and even cyanobacteria. This raises new questions about the structural and functional significance of highly-conserved C-terminal residues Tyr405, Trp413, Leu415, and Lys417 within the *fad6-3* deletion.

The first step in investigating the functional significance of the conserved residues is to successfully clone and heterologously express wild type *AtFAD6* in yeast with enough activity (18:2 production) to effectively evaluate and compare different constructs. Previous studies[86] suggested the activity of plastidial fatty acid desaturases expressed in yeast could be increased by deleting the chloroplast signal peptide and incorporating di-lysine (KEK) and ER retention (KKNL) motifs on the C-terminus, leading us to design the FAD6-KEK-KKNL construct used in this study. While previous studies examined the impact of ferredoxin co-expression on the activity of plastidial fatty acid desaturases expressed in yeast[87], the impact of the chloroplast signal peptide on the N-terminus of ferredoxin had not previously been tested. In this study, we evaluated the activity of FAD6-KEK-KKNL co-expressed with *AtFD2* with and without the transit peptide (T-FD2 and FD2, respectively) under the control of two different promoters: GAL1/10 (induced), and CDC11 (constitutive). We found the highest activity in yeast expressing FAD6-KEK-KKNL under the galactose induced promoter GAL1/10 and FD2 under the constitutive promoter CDC11. Activity was consistently higher when the FAD6 construct was under the control of the galactose induced promoter Gal1/10, but the results for the two different ferredoxin constructs (T-FD2 and FD2) were inconsistent when the promoters were switched, leading to the conclusion that the transit peptide does not have a notable effect on activity.

In conclusion, after identifying a novel allele of *AtFAD6*, we successfully designed a system for the heterologous expression of *AtFAD6* in *Saccharomyces cerevisiae* which resulted in enough activity (18:2 production) to effectively compare different constructs. We plan to use this yeast system to clone and express *fad6-1, fad6-2, and fad6-3* sequences in addition to *fad6* C-terminal truncations and other constructs to evaluate the impact of conserved residues on enzyme

function. In conducting this study, we hope to elucidate the function of the conserved residues, and expand knowledge about the molecular mechanisms and substrate specificity of integral membrane desaturases.

Table 2.1 *AtFAD6* allelic mutants

Allele	Genomic DNA	Amino Acid	Reference
fad6-1	G→A at bp1,075	G160R	54
fad6-2	C→T at bp1,425	P225S	24
fad6-3	G→A at bp2,353	Δ13(Y395-K407)	This Study

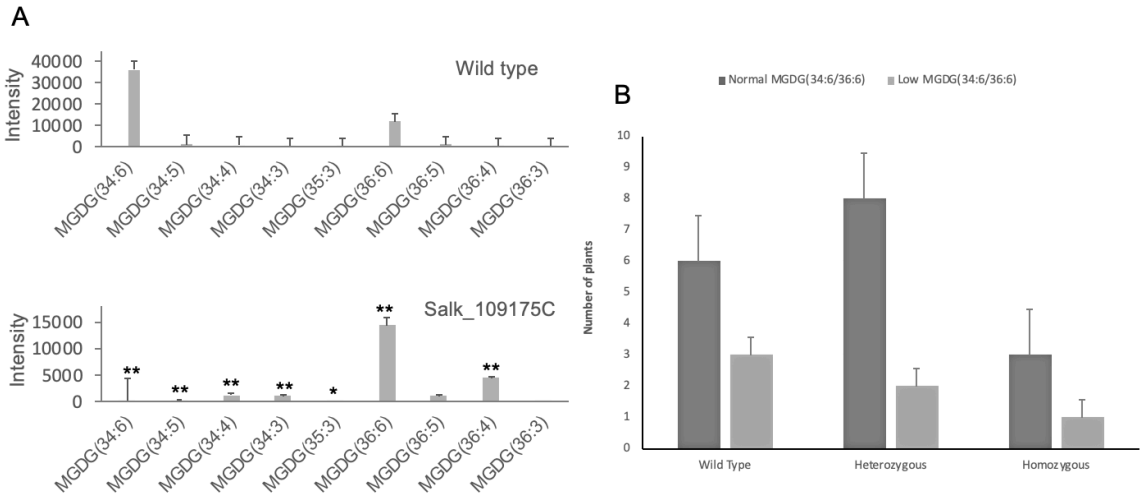

Figure 2.1 The lipid phenotype did not co-segregate with the *At5g64790* T-DNA insertional mutation in the F2 generation.

(A) Levels of monogalatosyldiacylglycerol (MGDG) lipid molecular species in leaves of 30-day old wild type (Col-0) and Salk_109175C plants. An amount of lipid extract corresponding to 0.04 mg of leaf dry weight was used for each sample. One asterisk indicates a p value of < 0.01 for comparison of the molecular species between wild-type and Salk_109175, while two asterisks indicates a p < 0.001. The ratio of MGDG(34:6)/MGDG(36:6) was 3 in leaves of wild-type plants (upper panel) and 0.001 in leaves of Salk_109175C plants. **(B)** Phenotypes of genotyped F2 plants from cross of wild type (Col-0) and Salk_109175C. Plants were genotyped for the Salk_109175C insertion in At5g64790, and ratios of plastidial MGDG species. The ratios of MGDG(34:6/36:6) in the genotyped plants were classified as "normal", which was a ratio greater than 1 or "low", a ratio less than 1. The Y-axis indicates the number of plants of each genotype with each phenotype.

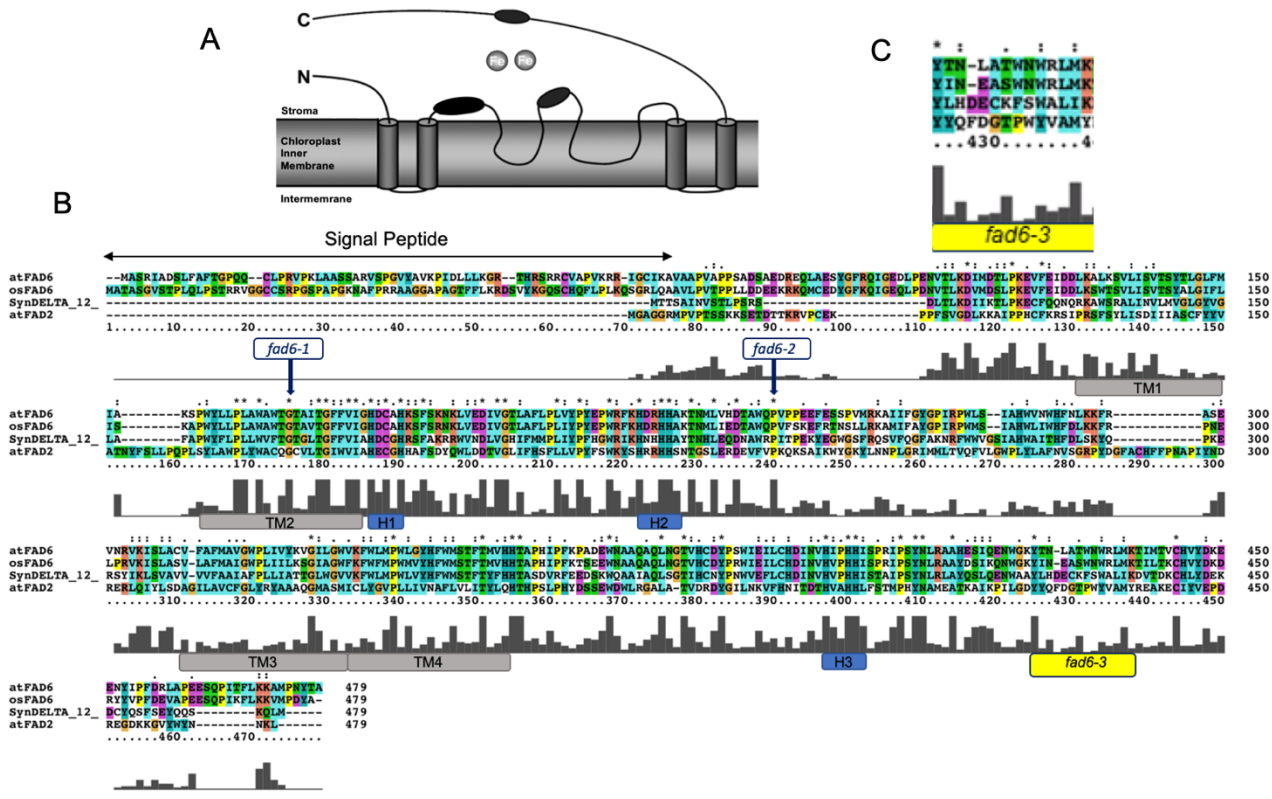

Figure 2.2 FAD6 has close homologs in other plants and cyanobacteria.

(A) Predicted structural model of FAD6 adapted from Zhang et al.[65] Three His boxes (black ellipses) coordinate two iron atoms (gray circles) at the active site. **(B)** Protein sequence alignments of ω6-desaturases from *Arabidopsis thaliana, Oryza sativa* (rice), and *Synechocystis* (cyanobacteria). Arabidopsis ω6-desaturases include the plastidial enzyme FAD6 and endoplasmic reticulum-localized FAD2. Alignment of amino acid sequences for ω6-desaturase proteins was done using the program Clustal X v.2.0[94] on the default setting. Amino acids affected by previously described *AtFAD6* mutations are indicated by blue arrows. Specific mutations are described in (Table 2.1). Yellow box indicates the 13AA region deleted in *fad6-3*. Grey bars beneath alignments indicate the degree of homology. **(C)** Enlargement of *fad6-3* deletion.

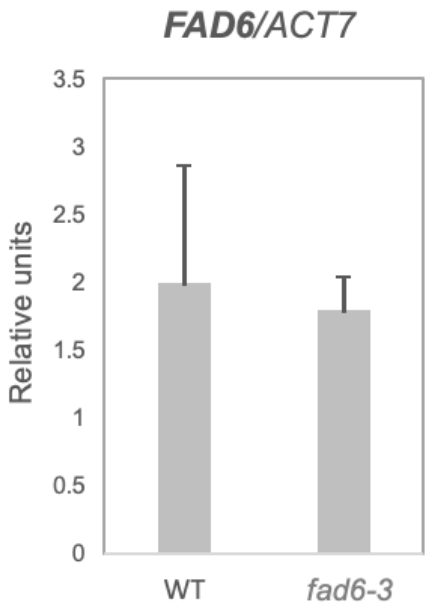

Figure 2.3 *FAD6* mRNA transcript levels are not affected in *fad6-3* mutants.

Quantitative real-time PCR (qRT-PCR) was performed with cDNA from the leaves of 30-day-old plants with *ACTIN 7* (*ACT7)* as the reference gene. The ratio of the expression of *FAD6* over the expression of *ACT7* is reported for each genotype. Error bars indicate standard deviations for the averages from 3 biological replicates.

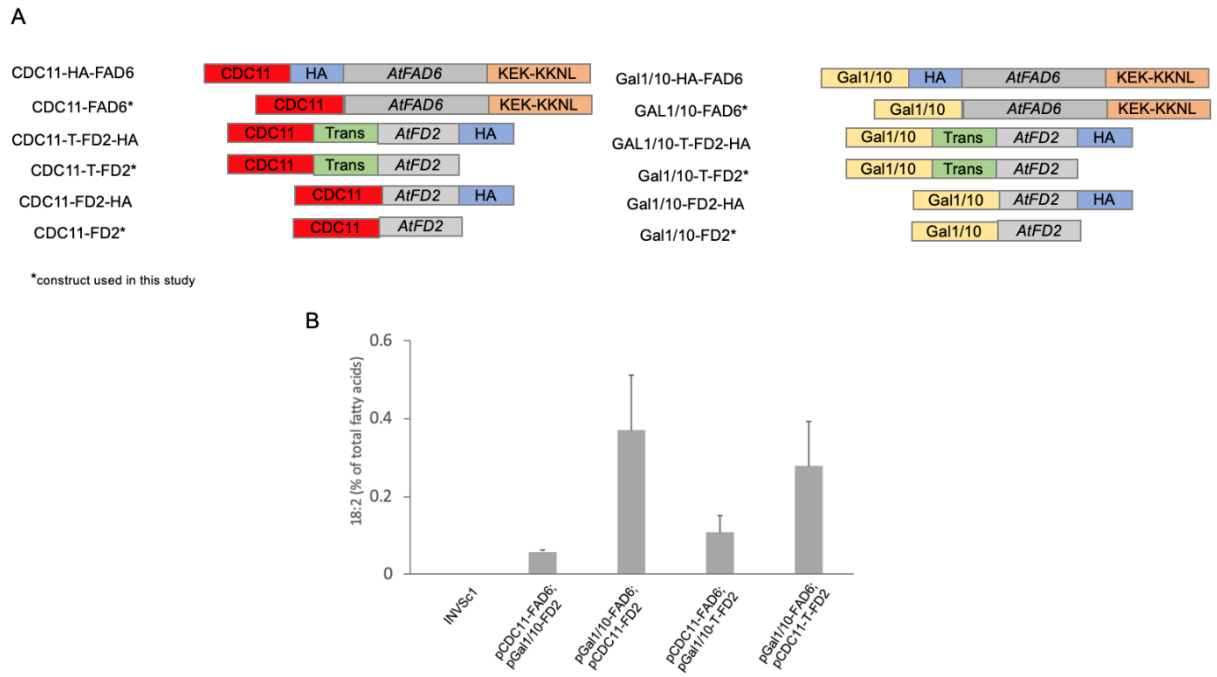

Figure 2.4 Expression of *FAD6* results in production of 18:2 in *Saccharomyces cerevisiae.* (A) Schematics of the constructs used in this study. *AtFAD6* refers to the Arabidopsis gene At5g30950 encoding *FAD6* with the first 207bp (transit signal) deleted. *AtFD2* refers to the Arabidopsis gene At3g12120 encoding photosynthetic ferredoxin *FD2* with the first 156bp (transit signal) deleted. Trans refers to the transit peptide endogenous to Arabidopsis *FD2* (first 156bp). KEK-KKNL was added to FAD6 construct for ER retention. HA refers to epitope tag. **(B)** Levels of 18:2 as a percent of total fatty acids measured from yeast strains of genotypes listed in Table S5.

Chapter 3 - Perspectives

The future of this project involves using the constructs and yeast expression system designed and tested in this study to clone and heterologously express *fad6-1, fad6-2, and fad6-3* sequences in addition to *fad6* C-terminal truncations and other constructs in yeast to evaluate the impact of conserved residues on enzyme activity. The Gal1/10-FAD6 construct described in the previous chapter will be used as the template for making additional mutant *FAD6* constructs, and co-expressing the new constructs with CDC11-FD2.

New constructs to be evaluated include single-base substitutions at conserved residues: Y405A, W413A, L415A, and K417A as well as the single base mutations described in previous studies on *fad6-1*[54] and *fad6-2*[6]. The *fad6-3* deletion mutant identified in this study will be cloned and expressed, in addition to two truncations aimed at evaluating whether the mutation causes structural changes that interfere with the active site; one truncation will have the last 27 amino acids deleted, the second truncation will have the last 54 amino acids deleted. The last three constructs involve: (1) replacing all four-conserved amino-acids with alanine at the same time (2) replacing the 13 amino acids deleted in *fad6-3* with the 14 amino acids from Synechocystis aligned with the deletion in Figure 2.2, and (3) replacing the 13 amino acids in *fad6-3* with the 14 amino acids from *AtFAD2* aligned with the deletion in Figure 2.2.

Protein structural modeling of the predicted secondary structure of wild type *at*FAD6, *fad6-3*, and *at*FAD6 mutant constructs 1-3 suggest the secondary structure of the *fad6-3* allelic mutant is notably different than wild type at the C-terminal end following the mutation. More specifically, it appears that there is the loss of a break between two alpha helices in the area of the deletion,

and a reduction of hydrophilicity of the C-terminus following the deletion (Figure S7). This break between alpha helices could be an area where the C-terminus turns, allowing the protein to fold in a conformation where the active site histidine boxes are in proximity to each other for catalytic activity. Protein structural modeling of constructs 1-3 indicate these structural characteristics are maintained to varying degrees in each of the constructs. If this is the case, then catalytic activity should be preserved to some extent, and we would expect yeast transformed with constructs 1-3 to make some 18:2. We would also expect to see activity in the 54 amino acid truncation, which includes the *fad6-3* deletion. On the other hand, if one of the conserved amino acids plays a functional role, production of 18:2 may not be seen construct 1, which contains the alanine substitutions, or the 54 amino acid truncation, but it would be observed in the 27 amino acid truncation and potentially in the other two constructs.

Although FAD6 is a major plant membrane lipid desaturase which is conserved across plant species and considered to be well annotated, little is known about key residues and interactions in the protein required for substrate specificity and catalytic activity, and only three allelic mutants have been reported. It is our hope that this work provides insight into the role of the C-terminus in the function of *at*FAD6, and expands our knowledge on the molecular mechanisms of integral membrane desaturases in general.

References

1. Alberts B, Johnson A, Lewis J, et al., eds. *The lipid bilayer.* 4th ed. New York: Garland Science; 2002 Molecular Biology of the Cell.

2. Fahy E, Cotter D, Sud M, Subramaniam S. Lipid classification, structures and tools. *BBA - Molecular and Cell Biology of Lipids*. 2011;1811(11):637-647. https://www.sciencedirect.com/science/article/pii/S1388198111000916. doi: 10.1016/j.bbalip.2011.06.009.

3. Kachroo P, Kachroo A, Lapchyk L, Hildebrand D, Klessig DF. Restoration of defective cross talk in ssi2 mutants: Role of salicylic acid, jasmonic acid, and fatty acids in SSI2-mediated signaling. *Mol Plant Microbe Interact*. 2003;16(11):1022-1029. doi: 10.1094/MPMI.2003.16.11.1022 [doi].

4. Shah J, Kachroo P, Nandi A, Klessig DF. A recessive mutation in the arabidopsis SSI2 gene confers SA- and NPR1-independent expression of PR genes and resistance against bacterial and oomycete pathogens. *Plant J*. 2001;25(5):563-574. doi: tpj992 [pii].

5. Kachroo P, Shanklin J, Shah J, Whittle EJ, Klessig DF. A fatty acid desaturase modulates the activation of defense signaling pathways in plants. *Proc Natl Acad Sci U S A*. 2001;98(16):9448-9453. doi: 10.1073/pnas.151258398 [doi].

6. Kachroo A, Lapchyk L, Fukushige H, Hildebrand D, Klessig D, Kachroo P. Plastidial fatty acid signaling modulates salicylic acid- and jasmonic acid-mediated defense pathways in the arabidopsis ssi2 mutant. *Plant Cell*. 2003;15(12):2952-2965. doi: 10.1105/tpc.017301 [doi].

7. Sekine KT, Nandi A, Ishihara T, et al. Enhanced resistance to cucumber mosaic virus in the arabidopsis thaliana ssi2 mutant is mediated via an SA-independent mechanism. *Mol Plant Microbe Interact*. 2004;17(6):623-632. doi: 10.1094/MPMI.2004.17.6.623 [doi].

8. Nandi A, Moeder W, Kachroo P, Klessig DF, Shah J. Arabidopsis ssi2-conferred susceptibility to botrytis cinerea is dependent on EDS5 and PAD4. *Mol Plant Microbe Interact*. 2005;18(4):363-370. doi: 10.1094/MPMI-18-0363 [doi].

9. Han X, Gross RW. Global analyses of cellular lipidomes directly from crude extracts of biological samples by ESI mass spectrometry: A bridge to lipidomics. *Journal of Lipid Research*. 2003;44(6):1071-1079. http://www.jlr.org/cgi/content/abstract/44/6/1071. doi: 10.1194/jlr.R300004-JLR200.

10. Weintraub ST, Pinckard RN, Hail M. Electrospray ionization for analysis of platelet-activating factor. *Rapid Commun Mass Spectrom*. 1991;5(7):309-311. doi: 10.1002/rcm.1290050702 [doi].

11. Duffin KL, Henion JD, Shieh JJ. Electrospray and tandem mass spectrometric characterization of acylglycerol mixtures that are dissolved in nonpolar solvents. *Anal Chem*. 1991;63(17):1781-1788. doi: 10.1021/ac00017a023 [doi].

12. Welti R, Wang X. Lipid species profiling: A high-throughput approach to identify lipid compositional changes and determine the function of genes involved in lipid metabolism and signaling. *Current Opinion in Plant Biology*. 2004;7(3):337-344. https://www.sciencedirect.com/science/article/pii/S1369526604000433. doi: 10.1016/j.pbi.2004.03.011.

13. B. Brugger, G. Erben, R. Sandhoff, F. T. Wieland, W. D. Lehmann. Quantitative analysis of biological membrane lipids at the low picomole level by nano-electrospray ionization tandem mass spectrometry. *Proceedings of the National Academy of Sciences of the United States of America*. 1997;94(6):2339-2344. https://www.jstor.org/stable/41639. doi: 10.1073/pnas.94.6.2339.

14. Devaiah SP, Roth MR, Baughman E, et al. Quantitative profiling of polar glycerolipid species from organs of wild-type arabidopsis and a phospholipase Dalpha1 knockout mutant. *Phytochemistry*. 2006;67(17):1907-1924. doi: S0031-9422(06)00321-9 [pii].

15. Welti R, Li W, Li M, et al. Profiling membrane lipids in plant stress responses. role of phospholipase D alpha in freezing-induced lipid changes in arabidopsis. *J Biol Chem*. 2002;277(35):31994-32002. doi: 10.1074/jbc.M205375200 [doi].

16. Welti R, Wang X, Williams TD. Electrospray ionization tandem mass spectrometry scan modes for plant chloroplast lipids. *Analytical Biochemistry*. 2003;314(1):149-152. https://www.sciencedirect.com/science/article/pii/S0003269702006231. doi: 10.1016/S0003-2697(02)00623-1.

17. Schwudke D, Schuhmann K, Herzog R, Bornstein SR, Shevchenko A. Shotgun lipidomics on high resolution mass spectrometers. *Cold Spring Harb Perspect Biol*. 2011;3(9):a004614. doi: 10.1101/cshperspect.a004614 [doi].

18. Xian F, Hendrickson CL, Marshall AG. High resolution mass spectrometry. *Anal Chem*. 2012;84(2):708-719. doi: 10.1021/ac203191t [doi].

19. Marshall AG, Hendrickson CL. High-resolution mass spectrometers. *Annu Rev Anal Chem (Palo Alto Calif)*. 2008;1:579-599. doi: 10.1146/annurev.anchem.1.031207.112945 [doi].

20. Nandi A, Kachroo P, Fukushige H, Hildebrand DF, Klessig DF, Shah J. Ethylene and jasmonic acid signaling affect the NPR1-independent expression of defense genes without impacting resistance to pseudomonas syringae and peronospora parasitica in the arabidopsis ssi1 mutant. *Mol Plant Microbe Interact*. 2003;16(7):588-599. doi: 10.1094/MPMI.2003.16.7.588 [doi].

21. Li Q, Shen W, Zheng Q, et al. Effects of eIFiso4G1 mutation on seed oil biosynthesis. *Plant J*. 2017;90(5):966-978. doi: 10.1111/tpj.13522 [doi].

22. Winter E, Brummel M, Schuch R, Spener F. Decarboxylation of malonyl-(acyl carrier protein) by 3-oxoacyl-(acyl carrier protein) synthases in plant fatty acid biosynthesis. *Biochem J*. 1997;321 (Pt 2)(Pt 2):313-318. doi: 10.1042/bj3210313 [doi].

23. Slabas AR, Fawcett T. The biochemistry and molecular biology of plant lipid biosynthesis. *Plant Mol Biol*. 1992;19(1):169-191.

24. Xu C, Moellering ER, Muthan B, Fan J, Benning C. Lipid transport mediated by arabidopsis TGD proteins is unidirectional from the endoplasmic reticulum to the plastid. *Plant & cell physiology*. 2010;51(6):1019-1028. https://www.ncbi.nlm.nih.gov/pubmed/20410050. doi: 10.1093/pcp/pcq053.

25. Browse J, Somerville C. GLYCEROLIPID SYNTHESIS: Biochemistry and regulation. *Annual Review of Plant Biology*. 1991;42(1):467-506. http://search.ebscohost.com/login.aspx?direct=true&scope=site&db=nlebk&db=nlabk&AN=195147.

26. Bates PD, Durrett TP, Ohlrogge JB, Pollard M. Analysis of acyl fluxes through multiple pathways of triacylglycerol synthesis in developing soybean embryos. *Plant Physiol*. 2009;150(1):55-72. doi: 10.1104/pp.109.137737 [doi].

27. Bates PD, Ohlrogge JB, Pollard M. Incorporation of newly synthesized fatty acids into cytosolic glycerolipids in pea leaves occurs via acyl editing. *J Biol Chem*. 2007;282(43):31206-31216. doi: M705447200 [pii].

28. Bates PD, Browse J. The significance of different diacylgycerol synthesis pathways on plant oil composition and bioengineering. *Front Plant Sci*. 2012;3:147. doi: 10.3389/fpls.2012.00147 [doi].

29. Williams JP, Imperial V, Khan MU, Hodson JN. The role of phosphatidylcholine in fatty acid exchange and desaturation in brassica napus L. leaves. *Biochem J*. 2000;349(Pt 1):127-133. doi: 10.1042/0264-6021:3490127 [doi].

30. Heinz E, Roughan PG. Similarities and differences in lipid metabolism of chloroplasts isolated from 18:3 and 16:3 plants. *PLANT PHYSIOLOGY*. 1983;72(2):273-279. http://www.plantphysiol.org/cgi/content/abstract/72/2/273. doi: 10.1104/pp.72.2.273.

31. Mongrand et al. The C16:3/C18:3 fatty acid balance in photosynthetic tissues from 468 plant species. *Phytochemisty*. 1998.

32. Shanklin J, Cahoon EB. Desaturation and related modifications of fatty acids1. *Annual review of plant physiology and plant molecular biology*. 1998;49:611. https://www.ncbi.nlm.nih.gov/pubmed/15012248.

33. Somerville C, Browse J. Dissecting desaturation: Plants prove advantageous. *Trends Cell Biol*. 1996;6(4):148-153. doi: 0962-8924(96)10002-7 [pii].

34. McKeon TA, Stumpf PK. Purification and characterization of the stearoyl-acyl carrier protein desaturase and the acyl-acyl carrier protein thioesterase from maturing seeds of safflower. *J Biol Chem*. 1982;257(20):12141-12147.

35. Lindqvist Y, Huang W, Schneider G, Shanklin J. Crystal structure of delta9 stearoyl-acyl carrier protein desaturase from castor seed and its relationship to other di-iron proteins. *EMBO J*. 1996;15(16):4081-4092.

36. Stukey JE, McDonough VM, Martin CE. The OLE1 gene of saccharomyces cerevisiae encodes the delta 9 fatty acid desaturase and can be functionally replaced by the rat stearoyl-CoA desaturase gene. *J Biol Chem*. 1990;269(33):20144-20149.

37. Shanklin J, Whittle E, Fox BG. Eight histidine residues are catalytically essential in a membrane-associated iron enzyme, stearoyl-CoA desaturase, and are conserved in alkane hydroxylase and xylene monooxygenase. *Biochemistry*. 1994;33(43):12787-12794. doi: 10.1021/bi00209a009 [doi].

38. Avelange-Macherel MH, Macherel D, Wada H, Murata N. Site-directed mutagenesis of histidine residues in the delta 12 acyl-lipid desaturase of synechocystis. *FEBS Lett*. 1995;361(1):111-114. doi: 0014-5793(95)00163-4 [pii].

39. Bloomfield DK, Bloch K. The formation of delta 9-unsaturated fatty acids. *J Biol Chem*. 1960;235:337-345.

40. Higashi S, Murata N. An in vivo study of substrate specificities of acyl-lipid desaturases and acyltransferases in lipid synthesis in synechocystis PCC6803. *PLANT PHYSIOLOGY*. 1993;102(4):1275-1278. http://www.plantphysiol.org/cgi/content/abstract/102/4/1275. doi: 10.1104/pp.102.4.1275.

41. Ehud M. Landau, Jurg P. Rosenbusch. Lipidic cubic phases: A novel concept for the crystallization of membrane proteins. *Proceedings of the National Academy of Sciences of the United States of America*. 1996;93(25):14532-14535. https://www.jstor.org/stable/41118. doi: 10.1073/pnas.93.25.14532.

42. Bai Y, McCoy JG, Levin EJ, Zhou M. X-ray structure of a mammalian stearoyl-coa desaturase-1. *Biophysical Journal*. 2015;108(2):534a. https://www.sciencedirect.com/science/article/pii/S0006349514041381. doi: 10.1016/j.bpj.2014.11.2926.

43. Lee KR, Lee Y, Kim EH, et al. Functional identification of oleate 12-desaturase and omega-3 fatty acid desaturase genes from perilla frutescens var. frutescens. *Plant Cell Rep*. 2016;35(12):2523-2537. doi: 10.1007/s00299-016-2053-4 [doi].

40. Mareike Hoffmann, Ellen Hornung, Silke Busch, et al. A small membrane-peripheral region close to the active center determines regioselectivity of membrane-bound fatty acid desaturases from

aspergillus nidulans. *Journal of Biological Chemistry*. 2007;282(37):26666. http://www.jbc.org/content/282/37/26666.abstract. doi: 10.1074/jbc.M705068200.

45. Quinn PJ. Effects of temperature on cell membranes. *Symp Soc Exp Biol*. 1988;42:237-258.

46. Eric R. Moellering, Bagyalakshmi Muthan, Christoph Benning. Freezing tolerance in plants requires lipid remodeling at the outer chloroplast membrane. *Science*. 2010;330(6001):226-228. https://www.jstor.org/stable/40931820. doi: 10.1126/science.1191803.

47. Chris Somerville. Direct tests of the role of membrane lipid composition in low-temperature-induced photoinhibition and chilling sensitivity in plants and cyanobacteria. *Proceedings of the National Academy of Sciences of the United States of America*. 1995;92(14):6215-6218. https://www.jstor.org/stable/2367813. doi: 10.1073/pnas.92.14.6215.

48. Hugly S, Somerville C. A role for membrane lipid polyunsaturation in chloroplast biogenesis at low temperature. *Plant Physiol*. 1992;99(1):197-202. doi: 10.1104/pp.99.1.197 [doi].

49. Vijayan P, Browse J. Photoinhibition in mutants of arabidopsis deficient in thylakoid unsaturation. *Plant Physiol*. 2002;129(2):876-885. doi: 10.1104/pp.004341 [doi].

50. Kanervo E, Tasaka Y, Murata N, Aro EM. Membrane lipid unsaturation modulates processing of the photosystem II reaction-center protein D1 at low temperatures. *Plant Physiology.* 1997;114(3):841-849. http://www.plantphysiol.org/cgi/content/abstract/114/3/841. doi: 10.1104/pp.114.3.841.

51. Meï C, Michaud M, Cussac M, et al. Levels of polyunsaturated fatty acids correlate with growth rate in plant cell cultures. *Scientific reports*. 2015;5(1):15207. https://www.ncbi.nlm.nih.gov/pubmed/26469123. doi: 10.1038/srep15207.

52. Román Á, Hernández M, Soria-García Á, et al. Non-redundant contribution of the plastidial FAD8 ω-3 desaturase to glycerolipid unsaturation at different temperatures in arabidopsis. *Molecular Plant*. 2015;8(11):1599-1611. https://www.sciencedirect.com/science/article/pii/S1674205215002671. doi: 10.1016/j.molp.2015.06.004.

53. Gfeller A, Liechti R, Farmer EE. Arabidopsis jasmonate signaling pathway. *Science signaling*. 2010;3(109):cm4. https://www.ncbi.nlm.nih.gov/pubmed/20159850. doi: 10.1126/scisignal.3109cm4.

54. Browse J, Kunst L, Anderson S, Hugly S, Somerville C. A mutant of arabidopsis deficient in the chloroplast 16:1/18:1 desaturase. *Plant Physiol*. 1989;90(2):522-529. doi: 10.1104/pp.90.2.522 [doi].

55. Falcone DL, Gibson S, Lemieux B, Somerville C. Identification of a gene that complements an arabidopsis mutant deficient in chloroplast omega 6 desaturase activity. *Plant Physiol*. 1994;106(4):1453-1459. doi: 106/4/1453 [pii].

56. Zhang JT, Zhu JQ, Zhu Q, Liu H, Gao XS, Zhang HX. Fatty acid desaturase-6 (Fad6) is required for salt tolerance in arabidopsis thaliana. *Biochem Biophys Res Commun*. 2009;390(3):469-474. doi: 10.1016/j.bbrc.2009.09.095 [doi].

57. Xu C, Fan J, Riekhof W, Froehlich JE, Benning C. A permease-like protein involved in ER to thylakoid lipid transfer in arabidopsis. *EMBO J*. 2003;22(10):2370-2379. doi: 10.1093/emboj/cdg234 [doi].

58. Carlsson AS, LaBrie ST, Kinney AJ, Von Wettstein-Knowles P, Browse J. A KAS2 cDNA complements the phenotypes of the arabidopsis fab1 mutant that differs in a single residue bordering the substrate binding pocket. *The Plant Journal*. 2002;29(6):761-770. https://onlinelibrary.wiley.com/doi/abs/10.1046/j.1365-313X.2002.01253.x. doi: 10.1046/j.1365-313X.2002.01253.x.

59. Wu J, Lightner J, Warwick N, Browse J. Low-temperature damage and subsequent recovery of fab1 mutant arabidopsis exposed to 2 degrees C. *Plant Physiol*. 1997;113(2):347-356. doi: 10.1104/pp.113.2.347 [doi].

60. Wu J, Browse J. Elevated levels of high-melting-point phosphatidylglycerols do not induce chilling sensitivity in an arabidopsis mutant. *Plant Cell*. 1995;7(1):17-27. doi: 10.1105/tpc.7.1.17 [doi].

61. Gao J, Wallis JG, Browse J. Mutations in the prokaryotic pathway rescue the fatty acid biosynthesis1 mutant in the cold. *Plant Physiol*. 2015;169(1):442-452. doi: 10.1104/pp.15.00931 [doi].

62. Kachroo A, Lapchyk L, Fukushige H, Hildebrand D, Klessig D, Kachroo P. Plastidial fatty acid signaling modulates salicylic acid- and jasmonic acid-mediated defense pathways in the arabidopsis ssi2 mutant. *Plant Cell*. 2003;15(12):2952-2965. doi: 10.1105/tpc.017301 [doi].

63. Maatta S, Scheu B, Roth MR, et al. Levels of arabidopsis thaliana leaf phosphatidic acids, phosphatidylserines, and most trienoate-containing polar lipid molecular species increase during the dark period of the diurnal cycle. *Front Plant Sci*. 2012;3:49. doi: 10.3389/fpls.2012.00049 [doi].

64. Yamada K, Lim J, Dale JM, et al. Empirical analysis of transcriptional activity in the arabidopsis genome. *Science*. 2003;302(5646):842-846. doi: 10.1126/science.1088305 [doi].

65. Zhang J, Liu H, Sun J, et al. Arabidopsis fatty acid desaturase FAD2 is required for salt tolerance during seed germination and early seedling growth. *PLoS One*. 2012;7(1):e30355. doi: 10.1371/journal.pone.0030355 [doi].

66. Okuley J, Lightner J, Feldmann K, Yadav N, Lark E, Browse J. Arabidopsis FAD2 gene encodes the enzyme that is essential for polyunsaturated lipid synthesis. *Plant Cell*. 1994;6(1):147-158. doi: 10.1105/tpc.6.1.147 [doi].

67. Matos AR, Hourton-Cabassa C, Cicek D, et al. Alternative oxidase involvement in cold stress response of arabidopsis thaliana fad2 and FAD3+ cell suspensions altered in membrane lipid composition. *Plant Cell Physiol*. 2007;48(6):856-865. doi: pcm061 [pii].

68. Broadwater JA, Whittle E, Shanklin J. Desaturation and hydroxylation. residues 148 and 324 of arabidopsis FAD2, in addition to substrate chain length, exert a major influence in partitioning of catalytic specificity. *J Biol Chem*. 2002;277(18):15613-15620. doi: 10.1074/jbc.M200231200 [doi].

69. Covello PS, Reed DW. Functional expression of the extraplastidial arabidopsis thaliana oleate desaturase gene (FAD2) in saccharomyces cerevisiae. *Plant Physiol*. 1996;111(1):223-226. doi: 111/1/223 [pii].

70. Caiveau O, Fortune D, Cantrel C, Zachowski A, Moreau F. Consequences of omega -6-oleate desaturase deficiency on lipid dynamics and functional properties of mitochondrial membranes of arabidopsis thaliana. *J Biol Chem*. 2001;276(8):5788-5794. doi: 10.1074/jbc.M006231200 [doi].

71. Miquel M, Browse J. Arabidopsis mutants deficient in polyunsaturated fatty acid synthesis. biochemical and genetic characterization of a plant oleoyl-phosphatidylcholine desaturase. *J Biol Chem*. 1992;267(3):1502-1509.

72. Browse J, McConn M, James D, Miquel M. Mutants of arabidopsis deficient in the synthesis of alpha-linolenate. biochemical and genetic characterization of the endoplasmic reticulum linoleoyl desaturase. *J Biol Chem*. 1993;268(22):16345-16351.

73. Yadav NS, Wierzbicki A, Aegerter M, et al. Cloning of higher plant omega-3 fatty acid desaturases. *Plant Physiol*. 1993;103(2):467-476. doi: 10.1104/pp.103.2.467 [doi].

74. Gao J, Ajjawi I, Manoli A, et al. FATTY ACID DESATURASE4 of arabidopsis encodes a protein distinct from characterized fatty acid desaturases. *Plant J*. 2009;60(5):832-839. doi: 10.1111/j.1365-313X.2009.04001.x [doi].

75. Browse J, McCourt P, Somerville CR. A mutant of arabidopsis lacking a chloroplast-specific lipid. *Science*. 1985;227(4688):763-765. doi: 227/4688/763 [pii].

76. Qiu X, Hong H, MacKenzie SL. Identification of a delta 4 fatty acid desaturase from thraustochytrium sp. involved in the biosynthesis of docosahexanoic acid by heterologous expression in saccharomyces cerevisiae and brassica juncea. *J Biol Chem*. 2001;276(34):31561-31566. doi: 10.1074/jbc.M102971200 [doi].

77. Iba K, Gibson S, Nishiuchi T, et al. A gene encoding a chloroplast omega-3 fatty acid desaturase complements alterations in fatty acid desaturation and chloroplast copy number of the fad7 mutant of arabidopsis thaliana. *J Biol Chem*. 1993;268(32):24099-24105.

78. Gibson S, Arondel V, Iba K, Somerville C. Cloning of a temperature-regulated gene encoding a chloroplast omega-3 desaturase from arabidopsis thaliana. *Plant Physiol*. 1994;106(4):1615-1621. doi: 106/4/1615 [pii].

79. Heilmann I, Mekhedov S, King B, Browse J, Shanklin J. Identification of the arabidopsis palmitoyl-monogalactosyldiacylglycerol delta7-desaturase gene FAD5, and effects of plastidial retargeting of arabidopsis desaturases on the fad5 mutant phenotype. *Plant Physiol*. 2004;136(4):4237-4245. doi: pp.104.052951 [pii].

80. Fan J, Xu C. Genetic analysis of arabidopsis mutants impaired in plastid lipid import reveals a role of membrane lipids in chloroplast division. *Plant Signal Behav*. 2011;6(3):458-460. doi: 14715 [pii].

81. Napier JA, Hey SJ, Lacey DJ, Shewry PR. Identification of a caenorhabditis elegans Delta6-fatty-acid-desaturase by heterologous expression in saccharomyces cerevisiae. *Biochem J*. 1998;330 (Pt 2)(Pt 2):611-614. doi: 10.1042/bj3300611 [doi].

82. Domergue F, Abbadi A, Ott C, Zank TK, Zahringer U, Heinz E. Acyl carriers used as substrates by the desaturases and elongases involved in very long-chain polyunsaturated fatty acids biosynthesis reconstituted in yeast. *J Biol Chem*. 2003;278(37):35115-35126. doi: 10.1074/jbc.M305990200 [doi].

83. Wada H, Schmidt H, Heinz E, Murata N. In vitro ferredoxin-dependent desaturation of fatty acids in cyanobacterial thylakoid membranes. *J Bacteriol*. 1993;175(2):544-547. doi: 10.1128/jb.175.2.544-547.1993 [doi].

84. Hitz WD, Carlson TJ, Booth JR, Kinney AJ, Stecca KL, Yadav NS. Cloning of a higher-plant plastid omega-6 fatty acid desaturase cDNA and its expression in a cyanobacterium. *Plant Physiol*. 1994;105(2):635-641. doi: 105/2/635 [pii].

85. Venegas-Caleron M, Muro-Pastor AM, Garces R, Martinez-Force E. Functional characterization of a plastidial omega-3 desaturase from sunflower (helianthus annuus) in cyanobacteria. *Plant Physiol Biochem*. 2006;44(10):517-525. doi: S0981-9428(06)00127-6 [pii].

86. Venegas-Caleron M, Beaudoin F, Garces R, Napier JA, Martinez-Force E. The sunflower plastidial omega3-fatty acid desaturase (HaFAD7) contains the signalling determinants required for targeting to, and retention in, the endoplasmic reticulum membrane in yeast but requires co-expressed ferredoxin for activity. *Phytochemistry*. 2010;71(10):1050-1058. doi: 10.1016/j.phytochem.2010.04.017 [doi].

87. Venegas-Caleron M, Youssar L, Salas JJ, Garces R, Martinez-Force E. Effect of the ferredoxin electron donor on sunflower (helianthus annuus) desaturases. *Plant Physiol Biochem*. 2009;47(8):657-662. doi: 10.1016/j.plaphy.2009.03.005 [doi].

88. Domergue F, Abbadi A, Ott C, Zank TK, Zahringer U, Heinz E. Acyl carriers used as substrates by the desaturases and elongases involved in very long-chain polyunsaturated fatty acids

biosynthesis reconstituted in yeast. *J Biol Chem*. 2003;278(37):35115-35126. doi: 10.1074/jbc.M305990200 [doi].

89. Domergue F, Spiekermann P, Lerchl J, et al. New insight into phaeodactylum tricornutum fatty acid metabolism. cloning and functional characterization of plastidial and microsomal delta12-fatty acid desaturases. *Plant Physiol*. 2003;131(4):1648-1660. doi: 10.1104/pp.102.018317 [doi].

90. Edwards K, Johnstone C, Thompson C. A simple and rapid method for the preparation of plant genomic DNA for PCR analysis. *Nucleic Acids Res*. 1991;19(6):1349. doi: 10.1093/nar/19.6.1349 [doi].

91. Lukowitz W, Gillmor CS, Scheible WR. Positional cloning in arabidopsis. why it feels good to have a genome initiative working for you. *Plant Physiol*. 2000;123(3):795-805. doi: 10.1104/pp.123.3.795 [doi].

92. Hou X, Li L, Peng Z, et al. A platform of high-density INDEL/CAPS markers for map-based cloning in arabidopsis. *Plant J*. 2010;63(5):880-888. doi: 10.1111/j.1365-313X.2010.04277.x [doi].

93. Khosla A, Paper JM, Boehler AP, Bradley AM, Neumann TR, Schrick K. HD-zip proteins GL2 and HDG11 have redundant functions in arabidopsis trichomes, and GL2 activates a positive feedback loop via MYB23. *Plant Cell*. 2014;26(5):2184-2200. doi: tpc.113.120360 [pii].

94. Larkin MA, Blackshields G, Brown NP, et al. Clustal W and clustal X version 2.0. *Bioinformatics*. 2007;23(21):2947-2948. doi: btm404 [pii].

95. Yang J, Yan R, Roy A, Xu D, Poisson J, Zhang Y. The I-TASSER suite: Protein structure and function prediction. *Nat Methods*. 2015;12(1):7-8. doi: 10.1038/nmeth.3213 [doi].

96. Yang J, Zhang Y. I-TASSER server: New development for protein structure and function predictions. *Nucleic Acids Res*. 2015;43(W1):174. doi: 10.1093/nar/gkv342 [doi].

97. Yang J, Zhang Y. Protein structure and function prediction using I-TASSER. *Curr Protoc Bioinformatics*. 2015;52:5.8.-15. doi: 10.1002/0471250953.bi0508s52 [doi].

98. Sambrook J, Fritsch EF, Maniatis T. *Molecular cloning.* 4. ed. ed. Cold Spring Harbor: Cold Spring Harbor Laboratory Press; 2012.

99. Sikorski RS, Hieter P. A system of shuttle vectors and yeast host strains designed for efficient manipulation of DNA in saccharomyces cerevisiae. *Genetics*. 1989;122(1):19-27.

100. Finnigan GC, Thorner J. Complex in vivo ligation using homologous recombination and high-efficiency plasmid rescue from saccharomyces cerevisiae. *Bio Protoc*. 2015;5(13). doi: e1521 [pii].

101. Bessa D, Pereira F, Moreira R, Johansson B, Queiros O. Improved gap repair cloning in yeast: Treatment of the gapped vector with taq DNA polymerase avoids vector self-ligation. *Yeast*. 2012;29(10):419-423. doi: 10.1002/yea.2919 [doi].

102. Kitazono AA. Improved gap-repair cloning method that uses oligonucleotides to target cognate sequences. *Yeast*. 2009;26(9):497-505. doi: 10.1002/yea.1680 [doi].

103. Muhlrad D, Hunter R, Parker R. A rapid method for localized mutagenesis of yeast genes. *Yeast*. 1992;8(2):79-82. doi: 10.1002/yea.320080202 [doi].

104. Goldstein AL, McCusker JH. Three new dominant drug resistance cassettes for gene disruption in saccharomyces cerevisiae. *Yeast*. 1999;15(14):1541-1553. doi: 10.1002/(SICI)1097-0061(199910)15:143.0.CO;2-K [pii].

105. Elble R. A simple and efficient procedure for transformation of yeasts. *BioTechniques*. 1992;13(1):18-20.

106. Serrano-Vega MJ, Venegas-Caleron M, Garces R, Martinez-Force E. Cloning and expression of fatty acids biosynthesis key enzymes from sunflower (helianthus annuus L.) in escherichia coli. *J Chromatogr B Analyt Technol Biomed Life Sci*. 2003;786(1-2):221-228. doi: S1570023202007675 [pii].

107. Luthria DL, Sprecher H. 2-alkenyl-4,4-dimethyloxazolines as derivatives for the structural elucidation of isomeric unsaturated fatty acids. *Lipids*. 1993;28(6):561-564.

108. Nandi A, Krothapalli K, Buseman CM, et al. Arabidopsis sfd mutants affect plastidic lipid composition and suppress dwarfing, cell death, and the enhanced disease resistance phenotypes resulting from the deficiency of a fatty acid desaturase. Plant Cell. 2003;15(10):2383-2398. doi: 10.1105/tpc.015529 [doi].

109. Vu HS, Shiva S, Roth MR, et al. Lipid changes after leaf wounding in arabidopsis thaliana: Expanded lipidomic data form the basis for lipid co-occurrence analysis. Plant J. 2014;80(4):728-743. doi: 10.1111/tpj.12659 [doi].

110. Xiao S, Gao W, Chen QF, et al. Overexpression of arabidopsis acyl-CoA binding protein ACBP3 promotes starvation-induced and age-dependent leaf senescence. Plant Cell. 2010;22(5):1463-1482. doi: 10.1105/tpc.110.075333 [doi].

Appendix A - Supplemental Data

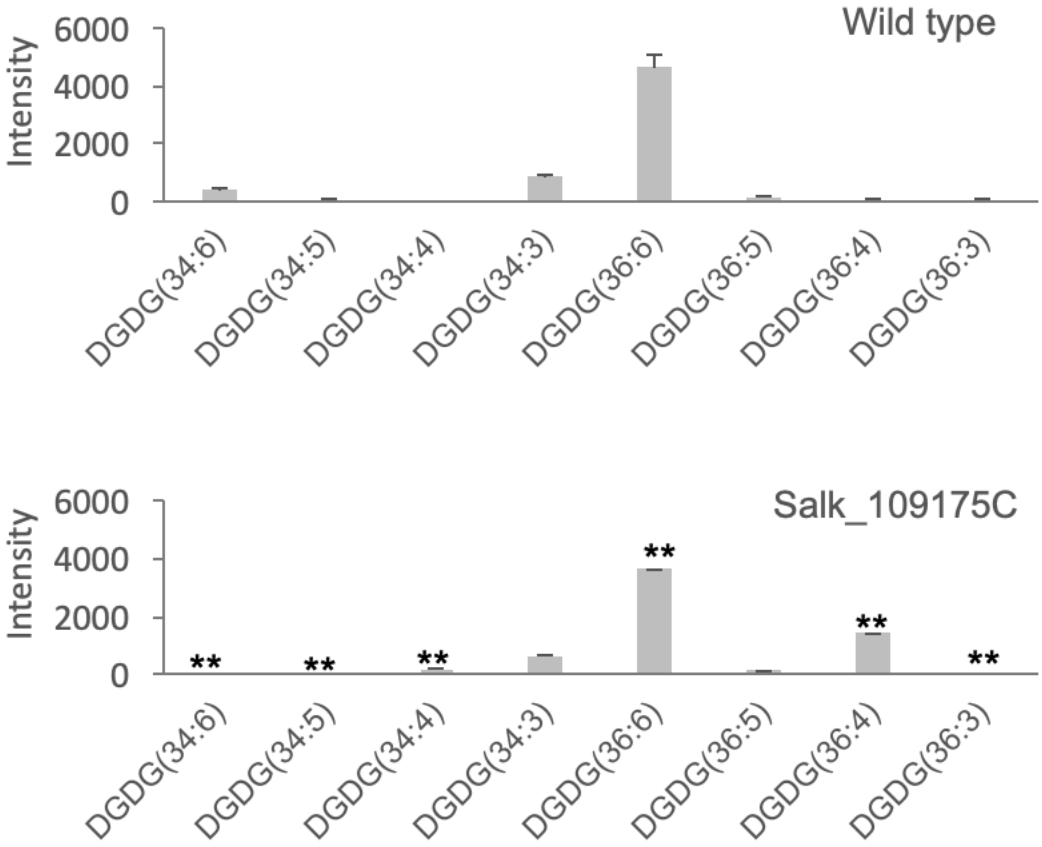

Figure S1 Levels of molecular species of digalactosyldiacylglycerol (DGDG) extracted from wild type (top, n = 6) and Salk_109175C (bottom, n = 18) leaf tissues. * indicates $p < 0.01$; ** indicates $p < 0.001$ for comparison between wild-type and Salk-109175C levels.

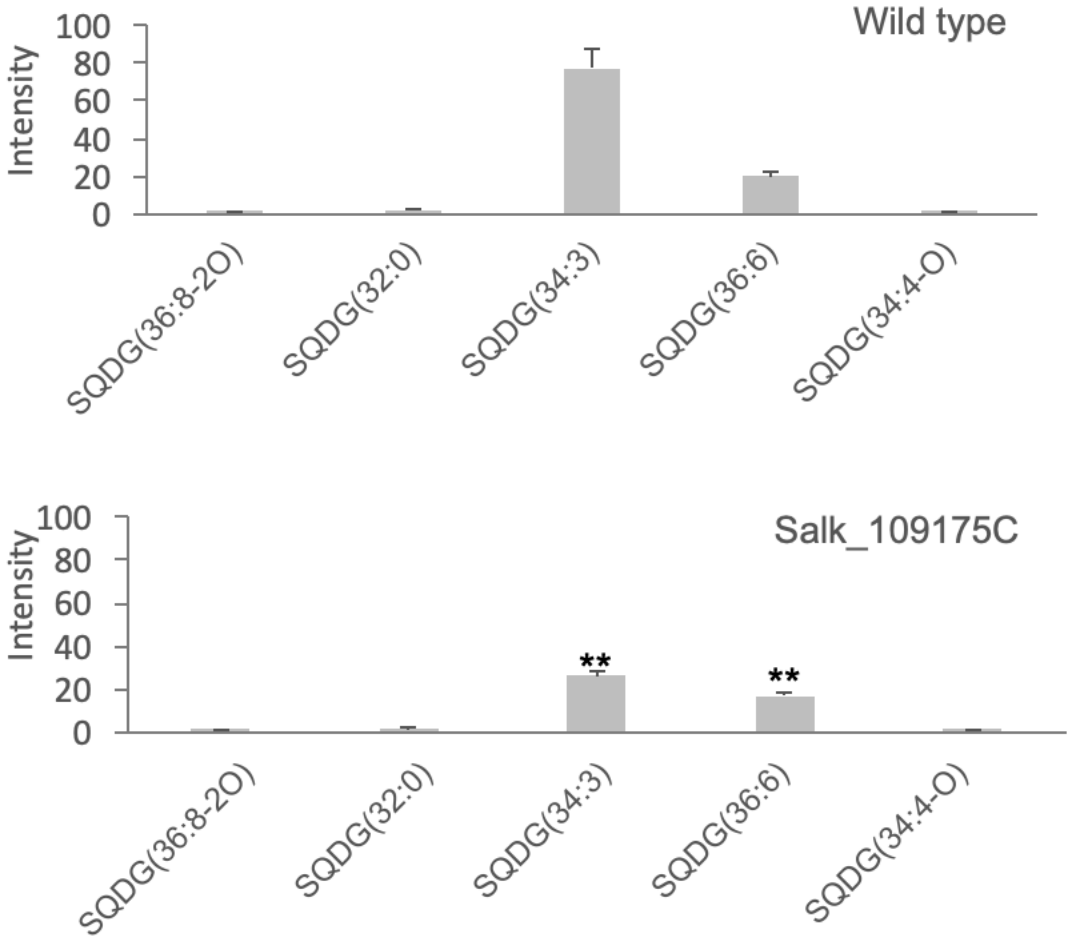

Figure S2 Levels of molecular species of sulfoquinovosyl diacylglycerol (SQDG) extracted from wild type (top, n = 6) and Salk_109175C (bottom, n = 18) leaf tissue. * indicates $p < 0.01$; ** indicates $p < 0.001$ for comparison between wild-type and Salk-109175C levels.

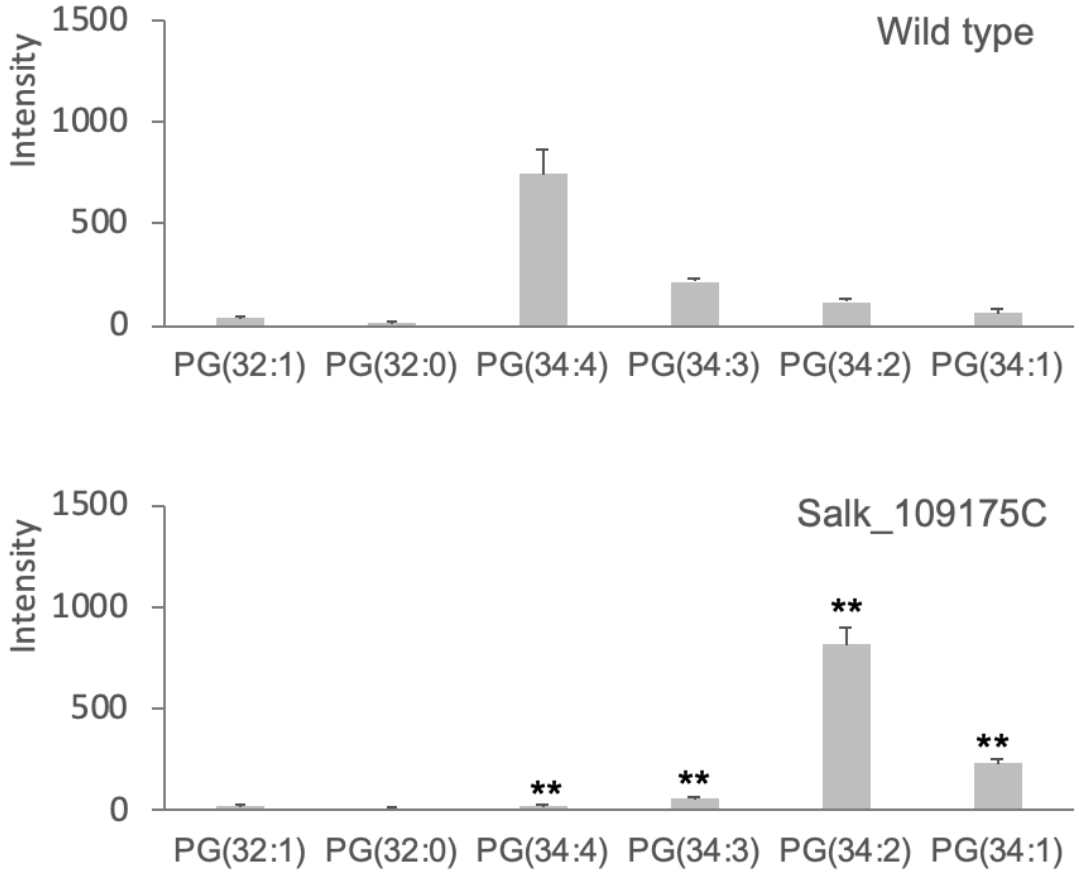

Figure S3 Levels of molecular species of phosphatidylglycerol (PG) extracted from wild type (top, n = 6) and Salk_109175C (bottom, n = 18) leaf tissue. * indicates $p < 0.01$; ** indicates $p < 0.001$ for comparison between wild-type and Salk-109175C levels.

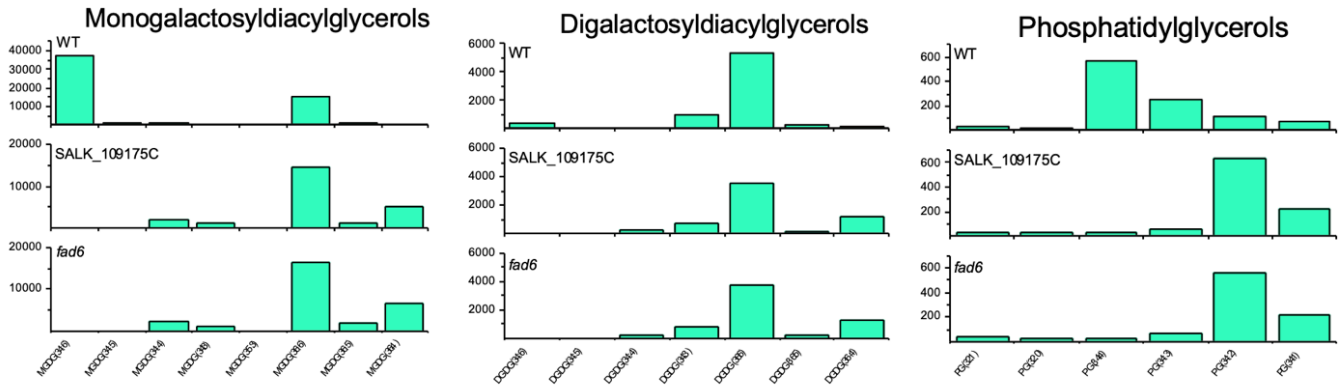

Figure S4 Levels of molecular species of monogalactosyldiacylglycerol (MGDG), digalactosyldiacylglycerol (DGDG), and phosphatidylglycerol (PG) extracted from wild type (top, n = 1), Salk_109175C (middle n = 1), and *fad6-1* (n=1) leaf tissue.

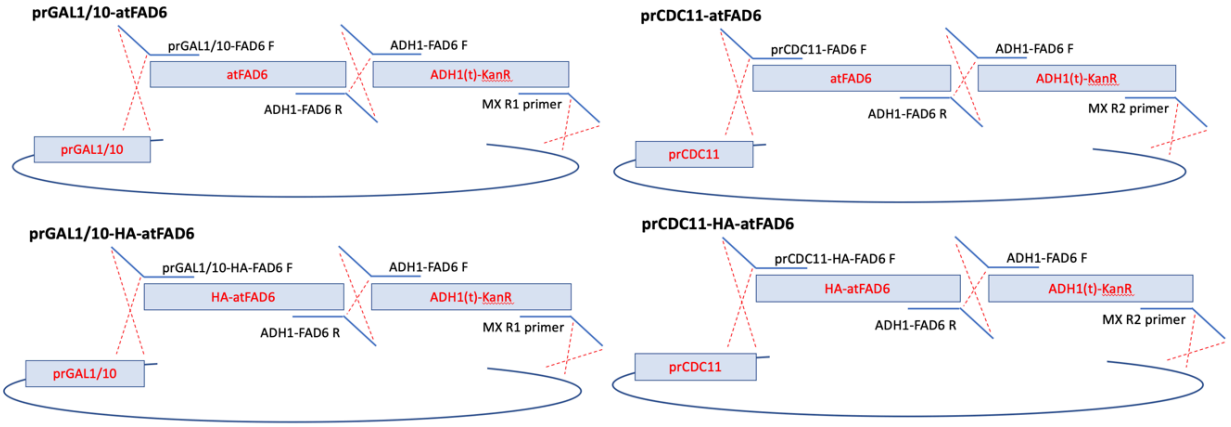

Figure S5 Visual representation of *atFAD6* plasmid assemblies.

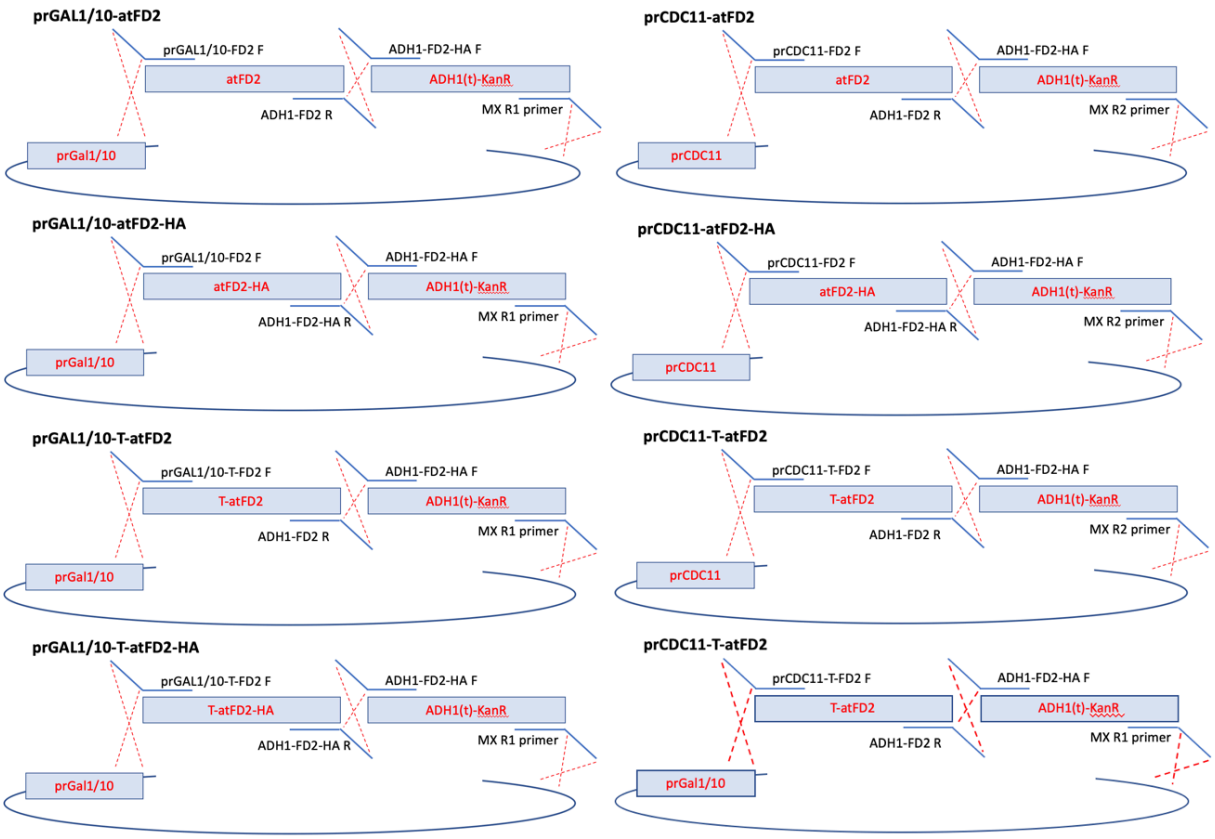

Figure S6 Visual representation of *atFD2* plasmid assemblies.

Figure S7 Protein structural modeling showing the predicted secondary structure of wild type *atFAD6*, *fad6-3*, and *atFAD6* mutant constructs 1-3. (1) all four-conserved amino-acids replaced with alanine at the same time, (2) 13 amino acids deleted in *fad6-3* replaced with the 14 amino acids from Synechocystis aligned with the deletion in Figure 2.2, and (3) the 13 amino acids deleted in *fad6-3* replaced with the 14 amino acids from *AtFAD2* aligned with the deletion in Figure 2.2. Protein structural modeling was done using I-TASSER (Iterative Threading ASSEmbly Refinement)[95-97].

Primer Name	Chr.	Sequence 5'→3'
1-AC011661-1259(Forward)	1	GATATTTGTTTTGCTAACAC
1-AC011661-1259(Reverse)	1	TAATAAAGTTCCAGCTTTGA
1-AC000375-7539(Forward)	1	GAATTCTGTAACATCCCATTTCC
1-AC000375-7539(Reverse)	1	GGTCTAATTGCCGTTGTTGC
2-AC006420-1312(Forward)	2	TAGTCTGAGCTTACCAATA
2-AC006420-1312(Reverse)	2	TTACCCTCGACTCGTAAC
2-AC005623-5887(Forward)	2	TCCGATTCGATTAAACTC
2-AC005623-5887(Reverse)	2	TTATTTCCTATTTCAAGACT
3-AB022217-2402(Forward)	3	ACCTGTTCAGTCTATGTTAC
3-AB022217-2402(Reverse)	3	GGGAATTATTAACATTATCA
3-AL132954-8728(Forward)	3	GAGCAACATTAAGGATAGAA
3-AL132954-8728(Reverse)	3	ATCTCATACTCATAATATGTAG
4-AL049482-3304(Forward)	4	ACCTGTTCAGTCTATGTTAC
4-AL049482-3304(Reverse)	4	GGGAATTATTAACATTATCA
4-AL023094-8912(Forward)	4	ACCCTAAAACAATGTCTCTT
4-AL023094-8912(Reverse)	4	TGCTAACATGGAAATTTGTC
4-Z97343-5268(Forward)	4	TTCGGAGAAAGAAACGACAT
4-Z97343-5268(Reverse)	4	ATGGAACTATTCAGGCATTA
4-AL078465-7217(Forward)	4	GCAACCGCTGCTGCTTTA
4-AL078465-7217(Forward)	4	AATATTTGGCTTTGCGTAGA
5-AB010070-0918(Forward)	5	CTCTGTTGGGGCAAAACC
5-AB010070-0918(Reverse)	5	GATGCTGGAGAGTAGCTTAG
5-AB009053-9339(Forward)	5	AAAAGGCGACTACTAGCA
5-AB009053-9339(Reverse)	5	GCCATTTATTTGGTCAAC

Table S1 List of primers used for map-based cloning.

Primer Name	Sequence 5'→3'
Salk_109175C-F	AGATTTCACCGGACAAGGAC
Salk_109175C-R	TCTTCCGAACACAAAGTTGATCC
LBb1.3	GGACCGCTTGCTGCAACT
FAD6 5'UTR-F	GCTGAAGAAGGTGAAGAGGTGAG
FAD6 3' UTR-R	GTGTTAGAGAAGCTCATCGCTTGG
FAD6seq1	CGGATTGCAATAATGATGAATGC
FAD6seq2	CGGCTTCACAGCATATACACC
FAD6seq3	GGTAAGCTCTCCTCCACTG
FAD6seq4	GGTGGCCACTGATCGTATAC
FAD6seq5	GGCTACATGGAACTGGCG
qPCRFAD6-F	GGACAGGAACTGCAATTACCGG
qPCRFAD6-R	GAGTACCCACAATGTCTTCCACC
ACT7-F [93]	TCGCACATGTACTCGTTTCGCTTTC
ACT7-R [93]	TCGAGAAGCAGCGAGAGAGAAAGATAGA

Table S2 List of primers used for sequencing, amplification, and qRT-PCR of *atFAD6* and *ACT7*.

Primer Name	Sequence 5'→3'
prCDC11-HA-FAD6 F	ACAAGGCCTAAAGTTGCTAACCACCAGCCATGTATCCATACGATGTTCCAGATTATGCTG
prGAL10-HA-FAD6 F	TACTTTAACGTCAAGGAGAAAAAACTATAATGTATCCATACGATGTTCCAGATTATGCTG
prCDC11-FAD6 F	CACAAGGCCTAAAGTTGCTAACCACCAGCCATGGTTGCTGCACCAGTTGCACCACCATCT
prGAL10-FAD6 F	ATACTTTAACGTCAAGGAGAAAAAACTATAATGGTTGCTGCACCAGTTGCACCACCATCT
prCDC11-FD2 F	CACAAGGCCTAAAGTTGCTAACCACCAGCCATGGCTTCAACTGCATTGTCTTCAGCTATC
prGAL10-FD2 F	ATACTTTAACGTCAAGGAGAAAAAACTATAATGGCTTCAACTGCATTGTCTTCAGCTATC
CDC11-T-FD2 F	CACAAGGCCTAAAGTTGCTAACCACCAGCCATGGCTTCAACTGCATTGTCTTCAGCTATC
Gal10_T_FD2 F	ATACTTTAACGTCAAGGAGAAAAAACTATAATGGCTTCAACTGCATTGTCTTCAGCTATC
ADH1-FAD6 F	CACAGCAAAAGAAAAGAAGAAAAATTTGTAAGGCGCGCCACTTCTAAATAAGCGAATTTC
ADH1-FAD6 R	ATTTAGAAGTGGCGCGCCTTACAAATTTTTCTTCTTTTCTTTTGCTGTGTAATTTGGCAT
ADH1-FD2 F	CGAAACACATAAGGAAGAAGATATTGTTTAAGGCGCGCCACTTCTAAATAAGCGAATTTC
ADH1-FD2 R	ATTTAGAAGTGGCGCGCCTTAAACAATATCTTCTTCCTTATGTGTTTCGATAGTAACATC
ADH1-FD2-HA F	TTATCCATACGATGTTCCAGATTACGCTTAAGGCGCGCCACTTCTAAATAAGCGAATTTC
ADH1-FD2-HA R	CTTATTTAGAAGTGGCGCGCCTTAAGCGTAATCTGGAACATCGTATGGATAAACAATATC
MX R1	GGTCGACGGTATCGATAAGCTTGATATCGAATTACTGGATGGCGGCGTTAGTATCGAATC
MX R2	ACGTTGTAAAACGACGGCCAGTGAATTGTAATAACTGGATGGCGGCGTTAGTATCGAATC

Table S3 List of primers used to amplify fragments for in vivo ligation.

Plasmid	Description	Reference
pRS315	CEN, LEU2	[99]
pRS316	CEN, URA3	[99]
prGAL1/10-*atFAD6*	pRS316 *atFAD6* ::KEK-KKNL	This study
prGAL1/10-HA-*atFAD6*	pRS316 HA ::*atFAD6* ::KEK-KKNL	This study
prCDC11-*atFAD6*	pRS315 *atFAD6* ::KEK-KKNL	This study
prCDC11-HA-*atFAD6*	pRS315 HA ::*atFAD6* ::KEK-KKNL	This study
prGAL1/10-*atFD2*	pRS316 *atFD2(53-148)*	This study
prGAL1/10-*atFD2-HA*	pRS316 *atFD2(53-148)*::HA	This study
prGAL1/10-T-*atFD2*	pRS316 *atFD2*	This study
prGAL1/10-T-*atFD2-HA*	pRS316 *atFD2* ::HA	This study
prCDC11-*atFD2*	pRS315 *atFD2(53-148)*	This study
prCDC11-*atFD2-HA*	pRS315 *atFD2(53-148)*::HA	This study
prCDC11-T-*atFD2*	pRS315 *atFD2*	This study
prCDC11-T-*atFD2-HA*	pRS315 *atFD2* ::HA	This study

Table S4 List of plasmids used in this study.

Strain	Genotype
INVSc1	MATα his3D1 leu2 trp1-289 ura3-52 MAT his3D1 leu2 trp1-289 ura3-52
CDC11-FAD6; Gal1/10-FD2	INVSc1; pRS315 *atFAD6* ::KEK-KKNL; pRS316 *atFD2(53-148)*
Gal1/10-FAD6; CDC11-FD2	INVSc1; pRS316 *atFAD6* ::KEK-KKNL; pRS315 *atFD2(53-148)*
CDC11-FAD6; Gal1/10-T-FD2	INVSc1; pRS315 *atFAD6* ::KEK-KKNL; pRS316 *atFD2*
Gal1/10-FAD6; CDC11-T-FD2	INVSc1; pRS316 *atFAD6* ::KEK-KKNL; pRS315 *atFD2*

Table S5 List of yeast strains used in this study.